Received: 7 October 2020 | Revised: 10 February 2021 | Accepted: 2 March 2021

DOI: 10.1111/bph.15445

RESEARCH PAPER

Optogenetic tools for manipulation of cyclic nucleotides functionally coupled to cyclic nucleotide-gated channels

Thilo Henß[1,2] | Jatin Nagpal[1,2,3] | Shiqiang Gao[4] | Ulrike Scheib[5,6] | Alessia Pieragnolo[7] | Alexander Hirschhäuser[1,2,8] | Franziska Schneider-Warme[9] | Peter Hegemann[5] | Georg Nagel[4] | Alexander Gottschalk[1,2]

[1]Buchmann Institute for Molecular Life Sciences, Goethe University, Frankfurt, Germany

[2]Institute of Biophysical Chemistry, Goethe University, Frankfurt, Germany

[3]APC Microbiome Ireland, University College Cork, Cork, Ireland

[4]Department of Neurophysiology, Institute of Physiology, Biocentre, Julius-Maximilians-University, Würzburg, Germany

[5]Institute for Biology, Experimental Biophysics, Humboldt-Universität zu Berlin, Berlin, Germany

[6]Lead Discovery, Protein Technology, NUVISAN ICB GmbH, Berlin, Germany

[7]Faculty of Pharmacy, University of Padova, Padova, Italy

[8]Institute for Physiology and Pathophysiology, Department of Molecular Cell Physiology, Philipps-University Marburg, Marburg, Germany

[9]University Heart Center, Medical Center – University of Freiburg and Faculty of Medicine, Institute for Experimental Cardiovascular Medicine, Freiburg, Germany

Correspondence
Alexander Gottschalk, Buchmann Institute for Molecular Life Sciences and Institute of Biophysical Chemistry, Goethe-University, Max-von-Laue Str. 15, D-60438 Frankfurt, Germany.
Email: a.gottschalk@em.uni-frankfurt.de

Background and Purpose: The cyclic nucleotides cAMP and cGMP are ubiquitous second messengers regulating numerous biological processes. Malfunctional cNMP signalling is linked to diseases and thus is an important target in pharmaceutical research. The existing optogenetic toolbox in *Caenorhabditis elegans* is restricted to soluble adenylyl cyclases, the membrane-bound *Blastocladiella emersonii* CyclOp and hyperpolarizing rhodopsins; yet missing are membrane-bound photoactivatable adenylyl cyclases and hyperpolarizers based on K^+ currents.

Experimental Approach: For the characterization of photoactivatable nucleotidyl cyclases, we expressed the proteins alone or in combination with cyclic nucleotide-gated channels in muscle cells and cholinergic motor neurons. To investigate the extent of optogenetic cNMP production and the ability of the systems to depolarize or hyperpolarize cells, we performed behavioural analyses, measured cNMP content in vitro, and compared in vivo expression levels.

Key Results: We implemented *Catenaria* CyclOp as a new tool for cGMP production, allowing fine-control of cGMP levels. We established photoactivatable membrane-bound adenylyl cyclases, based on mutated versions ("A-2x") of *Blastocladiella* and *Catenaria* ("Be," "Ca") CyclOp, as *N*-terminal YFP fusions, enabling more efficient and specific cAMP signalling compared to soluble bPAC, despite lower overall cAMP production. For hyperpolarization of excitable cells by two-component optogenetics, we introduced the cAMP-gated K^+-channel SthK from *Spirochaeta thermophila* and combined it with bPAC, BeCyclOp(A-2x), or YFP-BeCyclOp(A-2x). As an alternative, we implemented the *B. emersonii* cGMP-gated K^+-channel BeCNG1 together with BeCyclOp.

Abbreviations: Arch, *Halorubrum sodomense* archaerhodopsin-3; ATR, all-*trans* retinal; BeCNG1, *Blastocladiella emersonii* cyclic-nucleotide-gated channel; BeCyclOp, *Blastocladiella emersonii* guanylyl cyclase opsin; bPAC, *Beggiatoa* photoactivatable adenylyl cyclase; BWM, body wall muscle; CaCyclOp, *Catenaria anguillulae* guanylyl cyclase opsin; ChR2, channelrhodopsin-2; CNG, cyclic nucleotide-gated; CNGC, cyclic nucleotide-gated channel; cNMP, cyclic nucleoside-3′,5′-monophosphate; euPAC, *Euglena* photoactivatable adenylyl cyclase; GtACR, *Guillardia theta* anion channel rhodopsin; mb, membrane-bound; NCs, nucleotidyl cyclases; NpHR, *Natronomonas pharaonis* halorhodopsin; PAC, photoactivatable adenylyl cyclase; PGC, photoactivatable guanylyl cyclase; SthK, *Spirochaeta thermophila* cAMP-gated K^+ channel; SV, synaptic vesicle.

Present address
Jatin Nagpal, APC Microbiome Ireland, University College Cork, Cork, Ireland

Ulrike Scheib, Lead Discovery, Protein Technology, NUVISAN ICB GmbH, Berlin, Germany

Funding information
Deutsche Forschungsgemeinschaft (DFG), Grant/Award Numbers: CRC807, P11, SPP1926, EXC115

Conclusion and Implications: We established a comprehensive suite of optogenetic tools for cNMP manipulation, applicable in many cell types, including sensory neurons, and for potent hyperpolarization.

KEYWORDS
adenylyl cyclases, *Caenorhabditis elegans*, cyclic nucleotide-gated channels, guanylyl cyclases, neuromuscular system, optogenetics, rhodopsin

What is already known

- Impairment of cNMP signalling is linked to various diseases, such as neurodegeneration and cardiovascular disorders.

What this study adds

- In vivo test system for the characterization of photoactivatable nucleotidyl cyclases
- Optogenetic tools for cNMP production, coupled to CNG channels to de- or hyperpolarize cells

What is the clinical significance

- Implementing photoactivatable nucleotidyl cyclases to aid pharmaceutical research

1 | INTRODUCTION

Optogenetics enables the modulation of biological processes in a spatiotemporally highly defined manner within living cells and animals. To this end, photosensitive proteins are genetically targeted to specific cell types (Knopfel et al., 2010; Yizhar et al., 2011). Several optogenetic tools were developed for the manipulation of ionic currents across the plasma membrane (PM) as well as for the signalling molecules **cAMP** and **cGMP** (Gao et al., 2015; Ryu et al., 2010; Schroder-Lang et al., 2007; Stierl et al., 2011; Tanwar et al., 2018). Both nucleotides are ubiquitous second messengers, triggering various biological responses by activating, for example, protein kinases (**PKA** and **PKG**) or **cyclic nucleotide-gated channels** (CNGCs) (Podda & Grassi, 2014). In eukaryotic GPCR signalling, cAMP is generated predominantly by membrane-bound (mb) **ACs**, which are located in microdomains together with GPCRs, PK(A) and their targets (Bock et al., 2020; Cooper & Tabbasum, 2014). In rare cases, cAMP is created by soluble ACs (Buck et al., 1999). Likewise, cGMP formation is either catalysed by **membrane bound** or by **soluble GC**s (Lucas et al., 2000).

Recently, several photoactivatable ACs and GCs (PACs and PGCs, respectively) were characterized (Gao et al., 2015; Ryu et al., 2010; Scheib et al., 2015; Stierl et al., 2011). In *Caenorhabditis elegans*, the microbial PACs from *Euglena* (euPAC) and *Beggiatoa* (bPAC), as well as the synthetic phytochrome-linked cyclases IlaC22 k27 and PaaC were implemented for optogenetic cAMP generation (Etzl et al., 2018; Ryu et al., 2014; Steuer Costa et al., 2017; Weissenberger et al., 2011). All are soluble proteins; thus, they do not precisely mimic cAMP signalling as occurring in response to membrane-bound ACs. The fungal GC rhodopsin from *Blastocladiella emersonii*, called BeCyclOp (BeRhGC, BeGC1, RhoGC) is particular in combining a rhodopsin and a GC, yielding an efficient mbGC for optogenetic cGMP generation (Avelar et al., 2014, 2015; Gao et al., 2015; Scheib et al., 2015). Another fungal CyclOp from *Catenaria anguillulae* was characterized in *Xenopus* oocytes and rat hippocampal neurons (Gao et al., 2015; Scheib et al., 2018). CyclOps, alternatively termed as RhoGCs, facilitate research in sensory neurons, which often signal via cGMP (Bargmann, 2006).

Nucleotide specificity is determined by two to three key amino acids in the active site and can be interconverted. Thus, highly efficient light-regulated cyclases can be turned into enzymes of the corresponding other nucleotide specificity. Accordingly, BeCyclOp and CaCyclOp were converted into ACs by distinct mutations (Scheib et al., 2018), as was the AC domain of bPAC, mutated into a GC and termed bPGC or BlgC (Ryu et al., 2010). The utility of nucleotidyl cyclases (NC) extends beyond their primary function as enzymes, when they are combined with CNGCs, resulting in "two-component optogenetics" (see below), as opposed to normal applications of microbial rhodopsins: these are most often used as directly light-gated ion channels or pumps to depolarize (e.g., channelrhodopsin-2 [ChR2]) or hyperpolarize (e.g., *Natronomonas pharaonis* halorhodopsin [NpHR]) excitable cells (Chuong et al., 2014; Klapoetke et al., 2014), enabling investigations of basic mechanisms of synaptic transmission, or to decipher neuronal networks triggering behaviour (Han et al., 2009; Husson, Costa, et al., 2012; Oranth et al., 2018; Schultheis et al., 2011). In *C. elegans*, hyperpolarizing tools such as the proton pump archaerhodopsin-3 (Arch) from *Halorubrum sodomense*, NpHR, or the *Guillardia theta* anion channel rhodopsins (GtACRs) were established (Bergs et al., 2018; Chow et al., 2010; Husson, Liewald, et al., 2012; Zhang et al., 2007). However, no dedicated optogenetic tool for transport or facilitation of K^+ currents exists, with the exception of BLINK (Cosentino et al., 2015), which does not express in

C. elegans (our unpublished observations). To overcome some of these limitations, a two-component optogenetic silencing system comprising the *Spirochaeta thermophila* cAMP-gated K^+ channel (SthK) and bPAC was implemented in several model organisms, enabling a more physiological silencing of excitable cells (Beck et al., 2018; Bernal Sierra et al., 2018).

Here, we characterize bPGC and CaCyclOp for their ability to allow optogenetic cGMP generation by co-expressing them with the TAX-2/-4 excitatory CNG channel in body wall muscle (BWM) cells of *C. elegans*. Further, we generate mbPACs by mutation of mbPGCs, and characterize them with respect to their light-induced cAMP production. To this end, we express them in cholinergic motor neurons and BWM cells and assess their influence on different behaviours of the animal. We demonstrated that mbPACs were more efficient than soluble bPAC in evoking behaviour, despite considerably higher overall cAMP production by the latter. Possibly, mbPACs affect signalling in motor neurons better as they generate cAMP in close proximity to the PM. Moreover, we implemented two-component optogenetic systems for silencing, consisting of SthK co-expressed with bPAC or mbPACs, or the *Blastocladiella emersonii* CNG1 (BeCNG1) K^+ channel combined with BeCyclOp. We evaluated the properties of these tool combinations, as well as their ability to silence BWM cells and cholinergic neurons. Our work establishes a comprehensive optogenetic toolbox for cGMP and cAMP manipulations or K^+-fluxes in *C. elegans*.

2 | METHODS

2.1 | Molecular biology

To express the NCs in *C. elegans*, the promoters p*unc-17* (cholinergic neurons; in vivo driving expression of the vesicular Acetylcholine transporter), and p*myo-3* (expression in BWM, driving expression of myosin heavy chain A) were used. As fluorescence selection marker, fluorescence proteins were expressed under the control of the promoter p*myo-2* (expression in pharyngeal muscle; myosin heavy chain C).

The plasmids **pMS04** [pmyo-3::bPGC::SL2::mCherry] (RRID: Addgene_168172), **pMS05** [pmyo-3::bPAC::SL2::mCherry], **pJN55** [pmyo-3::tax-2::GFP], **pJN58** [pmyo-3::tax-4::GFP], and **pJN63** [pmyo-3::BeCyclOp::SL2::mCherry] (RRID:Addgene_168173) were described earlier (Gao et al., 2015; Woldemariam et al., 2019). The plasmid **pASH3** [pmyo-3::BeCNG1-YFP] (RRID:Addgene_168167) was produced by amplification of the BeCNG1 cDNA fragment using primers BeCNG1_fwd (5′-CCGGGGATCCGCCACCATGGCTGTTGA-3′) and BeCNG1_rev (5′-GCTATAGGTACCTTCTCGAGATCCTCTTCAGGC ACA-3′) and subcloning into the pmyo-3::YFP vector using *BamH*I and *Kpn*I. For **pJN67** [punc-17::BeCyclOp::SL2::mCherry], the *unc-17* promoter was amplified with primers oJN197 (5′-CCTTTTGCT CACATGGGATTACACCAATCATTTC-3′) and oJN198 (5′-TGTCC TTCATTCTAGCTGAAAATTAAATATTTTAGTG-3′) and inserted into the BeCyclOp::SL2::mCherry vector via "in-fusion cloning." To construct **pJN68** [punc-17::BeCyclOp(A-3x)::SL2::mCherry], site-directed mutagenesis was conducted using primers oJN210 (5-′CTACAA GGTCAAAACCATCGGAGACGC-3′), oJN211 (5′-ACTCCCCAACGCT TGGCG-3′), oJN212 (5′-GACACTCGTCGGAGACACCGTC-3′), and oJN213 (5′-CAATCTGGGTTGAGGTCTCCGAG-3′). Plasmid **pJN69** [pmyo-3::BeCyclOp(A-3x)::SL2::mCherry] was generated by restriction digestion of pJN68 using *Kpn*I and *BspM*I and subcloning into the pmyo-3::BeCyclOp::SL2::mCherry backbone. To generate **pTH01** [pmyo-3::CaCyclOp(A-2x)::SL2::mCherry] and **pTH02** [pmyo-3:: CaCyclOp::SL2::mCherry], the respective CaCyclOp cDNA fragments were amplified with primers oTH5 (5′-GGCGCTCTAGAATGTCTA TGAAAGATAAAG-3′) and oTH6 (5′-GCGGTACCTTACTTTCTAGC GGTCAC-3′) and inserted into pmyo-3::SL2::mCherry vector using *Xba*I and *Kpn*I. **pTH04** [punc-17::CaCyclOp(A-2x)::SL2::mCherry] was produced by amplification of CaCyclOp(A-2x) fragment using primers oTH37 (5′-TCGGCTAGCCCATGTCTATGAAAGATAAAG-3′) and oTH6 (5′-GCGGTACCTTACTTTCTAGCGGTCAC-3′) and subcloning into punc-17::SL2::mCherry backbone using *Nhe*I and *Kpn*I. To construct **pTH11** [punc-17::BeCyclOp(A-2x)::SL2::mCherry], BeCyclOp fragment was amplified with primers oTH38 (5′-CAACCCACACTGGG ACCTCGTCGGAGACAC-3′) and oTH39 (5′-GTGTCTCCGACGAGGTC CCAGTGTGGGTTG-3′) and inserted into punc-17::BeCyclOp [E497K]::SL2::mCherry vector using *Bcl*I and *Kpn*I. For **pTH12** [pmyo-3::BeCyclOp(A-2x)::SL2::mCherry], the BeCyclOp(A-2x) fragment was amplified using primers oTH01 (5′-GCCGTCTAGAATGAAGGACAAG GACAACAACC-3′) and oTH04 (5′-AGCCGGTACCTTACTTACGTCC GAGGACCC-3′) and subcloned into pmyo-3::SL2::mCherry backbone using *Xba*I and *Kpn*I. To generate **pTH18** [pmyo-3::SthK-mCherry], the SthK-mCherry fragment was amplified using primers oTH50 (5′-CCA TCTAGAATGAAAAGCTCCGCC-3′) and oTH51 (5′-CACCTTGTAGA TGAAC-3′) and inserted into the pmyo-3::mCherry vector using *Xba*I and *Sbf*I. The plasmid **pTH20** [pmyo-3::SthK::SL2::GFP] was created by amplification of the SthK fragment using primers oTH50 (5′-CCATCTAGAATGAAAAGCTCCGCC-3′) and oTH52 (5′-ATGGTACC TTATCCCCGCCGTGATG-3′) and subcloning into pmyo-3::SL2::GFP backbone using *Xba*I and *Kpn*I. To construct **pTH21** [punc-17::SthK-mCherry], the SthK-mCherry fragment was obtained by digestion with *Nhe*I and *Sbf*I and inserted into the punc17::mCherry vector. For **pTH23** [punc-17::SthK::SL2::GFP], the SthK fragment was amplified with primers oTH53 (5′-ATGCTAGCATGAAAAGCTCCGC-3′) and oTH52 (5′-ATGGTACCTTATCCCCGCCGTGATG-3′) and subcloned into punc-17::SL2::mCherry backbone using *Nhe*I and *Kpn*I. The SL2:: mCherry fragment was exchanged with SL2::GFP using *Kpn*I and *Apa*I. **pTH32** [pmyo-3::YFP-CaCyclOp(A-2x)::SL2::mCherry] (RRID: Addgene_168168) was generated by amplifying YFP fragment with primers oTH69 (5′-ACGACCACTAGATCCATCTAGAATGGTGAGCAA GGGCGAGGAG-3′) and oTH71 (5′-CTTTATCTTTCATAGACATTGAT CCCTTGTACAGCTCGTCCATGCC-3′) and CaCyclOp(A-2x) fragment with primers oTH72 (5′-GGACGAGCTGTACAAGGGATCAATGTCTA TGAAAGATAAAG-3′) and oTH12 (5′-GACAAGCAGTTAACTAGGTG-3′), followed by insertion into the pmyo-3::SL2::mCherry vector via Gibson assembly. To construct **pTH33** [pmyo-3::YFP-BeCyclOp(A-2x)::SL2::mCherry] (RRID:Addgene_168169), the YFP fragment was amplified with primers oTH69 (5′-ACGACCACTAGATCCATCTAG AATGGTGAGCAAGGGCGAGGAG-3′) and oTH70 (5′-

GTTGTCCTTGTCCTTCATTGATCCCTTGTACAGCTCGTCCATG-3′) and the BeCyclOp(A-2x) fragment with primers oTH56 (5′-ATGAAGGACAAGGACAACAAC-3′) and oTH12 (5′-GACAAGCAG TTAACTAGGTG-3′). Subsequently, the fragments were inserted into the pmyo-3::SL2::mCherry backbone via Gibson assembly. **pTH41** [punc-17::YFP-BeCyclOp(A-2x)::SL2::mCherry] (RRID:Addgene_168170) and **pTH42** [punc-17::YFP-CaCyclOp(A-2x)::SL2::mCherry] (RRID:Addgene_168171) were generated by amplification of the YFP-CyclOp(A-2x) fragments using oTH81 (5′-CGGCTAGCATGGT GAGCAAGGG-3′) and oTH12 (5′-GACAAGCAGTTAACTAGGTG-3′). Subsequently, the fragments were subcloned into punc-17::SL2::mCherry backbone using *Nhe*I and *Kpn*I.

2.2 | *C. elegans* culture and transgenic animals

Cultivation was on nematode growth medium (NGM) in the presence of the *Escherichia coli* strain OP50-1 according to standard methods (Brenner, 1974). The *C. elegans* strains used or generated in this work are listed in Table S1.

Transgenic *C. elegans* were obtained by microinjection of DNA into the gonads of nematodes by standard procedures (Fire, 1986). The strain *lite-1(ce314)*, which lacks the intrinsic photophobic response, was used as background strain (Edwards et al., 2008). For ZX1741, 5.5 ng·µl^{-1} of pJN55 and pJN58 and 2 ng·µl^{-1} of pmyo-2::mCherry were microinjected. To create ZX2316, ZX2400-ZX2406, and ZX2609-2616, 15 ng·µl^{-1} of the plasmids pJN69, pJN63, pMS04, pTH02, pTH12, pTH33, pTH01, and pTH32 were injected. ZX2408 and ZX2617 were generated by injection of 7.5 ng·µl^{-1} of pMS05. The strains ZX1940, ZX1941, ZX2154, and ZX2391 were created by injection of 30 ng·µl^{-1} of pJN67, pJN68, pTH04, and pTH11. For ZX2326, 40 ng·µl^{-1} of pASH3 and 15 ng·µl^{-1} of pJN63 were microinjected. To generate ZX2398 and ZX2399, 10 ng·µl^{-1} of pTH18 and pTH21 and 1.5 ng·µl^{-1} of pmyo-2::CFP were microinjected. ZX2393 was produced by injection of 5.5 ng·µl^{-1} of pTH20 and 1.5 ng·µl^{-1} pmyo-2::mCherry. The strains ZX2504–ZX2507 were created by injection of 15 ng·µl^{-1} of pJN63, pTH12, pJN69, and pTH01. For ZX2394, 7.5 ng·µl^{-1} of pMS05 were microinjected. To create ZX2395, 5.5 ng·µl^{-1} of pTH23 and 3 ng·µl^{-1} pmyo-3::mCherry were injected. ZX2530 was generated by injection of 60 ng·µl^{-1} of pJN69. For ZX2606, 2.5 ng·µl^{-1} pTH23 and 100 ng·µl^{-1} pJN68 were microinjected. To obtain ZX2607 and ZX2608, 1 ng·µl^{-1} pTH23 and 30 ng·µl^{-1} pJN68 or 15 ng·µl^{-1} pTH11 were injected. For ZX2659 and ZX2660, 30 ng·µl^{-1} of pTH41 or pTH42 and 1.5 ng·µl^{-1} of pmyo-2::mCherry were used. For ZX2796 and ZX2797, 15 ng·µl^{-1} of pTH41 and 0.01 ng·µl^{-1} or 0.1 ng·µl^{-1} pTH23 were injected. ZX2798 was created by injection of 0.05 ng·µl^{-1} pTH23 and 30 ng·µl^{-1} pTH41.

2.3 | Fluorescence microscopy

Transgenic animals were immobilized on 2% agarose pads in M9 buffer (20-mM K_2HPO_4; 40-mM Na_2HPO_4; 80-mM NaCl; 1-mM $MgSO_4$) using 50-mM NaN_3 in H_2O. Expression was observed on an AxioScope.A1 (Zeiss, Germany) equipped with a 50-W (HBO) mercury lamp and *Natronomonas* halorhodopsin (NpHR) or green fluorescent protein (GFP) specific excitation/emission filter sets (AHF Analysentechnik, Germany). Images were obtained with a Hamamatsu ORCA-Flash 2.8 digital camera. For determination of protein expression level, z-stacks (0.3-µm intervals) were acquired under 10× magnification on a Zeiss Cell Observer Spinning Disk Confocal Microscope (Zeiss, Germany), using a 514-nm excitation laser at 40% power, a Rolera EM-C2 with EM Gain of 150, full resolution, and 100-ms exposure time. Images were exported as 16 bit czi files. Using ImageJ ([ImageJ, RRID:SCR_003070] version 1.52i), z-projections of the respective stacks were generated, and regions of interest (ROIs) were drawn along the whole body of the animal to measure the mean fluorescence intensity.

2.4 | *C. elegans* behavioural assays

Transgenic strains were kept in the dark on standard NGM plates (5.5-cm diameter; 8-ml NGM) with OP50-1 bacteria at room temperature. For behavioural assays, transgenic L4 larvae were selected for fluorescence under a Leica MZ16F dissection scope and transferred to freshly seeded plates and kept in the dark. Animals supplemented with **all-trans retinal (ATR)** were transferred to plates with OP50-1 containing 200-µM ATR. Measurements of the body length were performed as described previously (Liewald et al., 2008). Young adult animals were individually placed under red light (>600 nm) on plain NGM plates and assayed on an AxioScope.A1 microscope (Zeiss, Germany) with a 10× objective and transmission light filtered through a red 675 ± 50 nm bandpass filter. For colour illumination, the light of a 50-W HBO lamp was channelled through excitation bandpass filters of 470 ± 40 nm or 530 ± 50 nm with intensities of 0.1, 0.2, 0.4, 0.9, or 2.1 mW·mm^{-2}. Intensity was measured using a S120UV Sensor with PM 100D power meter (Thorlabs, Dachau, Germany). Video recordings of worms were done using a Canon G9 powershot camera. The duration of illumination was defined by a computer-controlled shutter (Sutter Instruments, USA). The body length values were calculated using a custom-made workflow in KNIME (KNIME, RRID:SCR_006164) version2.10 (Warr, 2012). Here, the length was normalized to the averaged values measured before illumination (0–5 s), and normalization was carried out for each worm. All the values below 80% or above 120% were excluded, and the length profiles were averaged for each strain. Swimming behaviour was analysed in a 96-well microtiter plate containing 100 µl of NGM and 50 µl of M9 buffer per well. Young adult animals were transferred to the microtiter plate under red light (650/50 nm) and adapted for 10 min in the dark. Video acquisition was performed with a Canon G9 powershot camera on a Axio Scope.A1 microscope (Zeiss, Germany). Animals were illuminated with a 50-W HBO lamp (Carl Zeiss AG, Germany, 470/40 nm, 530 ± 50 nm 0.1, 0.2, 0.4, 1, or 1.35 mW·mm^{-2}) and 4× magnification. Stimulation protocol was 30 s in darkness, 30 s in light, and if necessary 30, 60, or 270 s in darkness. Swimming cycles were counted for defined time periods of 15 or 30 s.

Locomotion behaviour analysis on NGM plates was performed using a worm tracker as previously described (Stirman et al., 2011). A mechanical shutter (Sutter Instruments, USA) was placed between the projector and the microscope and synchronized to the light protocol. Further, the transmission light was filtered through a red 675 ± 50 nm bandpass filter, and the intensity was measured using a S120UV Sensor with PM 100D power meter. Young adult animals were placed individually on NGM plates under red light (>600 nm) and kept for 15 min in the dark before the transfer to the worm tracker. The light protocol was 15 s dark/25 s light/and 15 s dark using a light intensity of 0.2 $mW{\cdot}mm^{-2}$ at 470/10 nm. Speed, bending angle, and body length values were calculated using a custom-made workflow in KNIME as previously described (Steuer Costa et al., 2017). Speed values >1.25 mm/s and length values which depicted deviations >25% with respect to the mean first 5 s of the video were excluded. Videos containing >15% of discarded data points were excluded. Speed, bending angle, and body length values of each animal were normalized to the averaged values measured before illumination (0–15 s).

2.5 | cNMP measurements using *C. elegans* extract

For *C. elegans* extract preparation, transgenic L4 larvae were selected for fluorescence under a Leica MZ16F dissection scope and transferred to freshly seeded OP50-1 plates containing 200-μM ATR and kept in the dark; 60 young adult animals were transferred under red light (>600 nm) into an Eppendorf tube containing 50-μl M9 buffer and 1-mM **3-isobutyl-1-methylxanthine (IBMX**, a phosphodiesterase blocker). Control animals (dark condition) were placed for 30 s or 15 min on an AxioScope.A1 microscope (Zeiss, Germany) with a 4× objective and transmission light filtered through a red 675 ± 50 nm bandpass filter. For colour illumination, the light of a 50-W HBO lamp was channelled through excitation bandpass filters of 470 ± 40 nm with an intensity of 0.5 $mW{\cdot}mm^{-2}$ for 30 s or 15 min. Subsequently, the animals were subjected to three freeze–thaw cycles using liquid nitrogen. Next, the animals were vortexed with 0.25- to 0.5-mm glass beads for 5 min. The supernatant after centrifugation (2000 rpm, 1 min) was used for measurement of the cNMP content. cAMP was measured using AlphaScreen cAMP Detection Kit (PerkinElmer), whereas cGMP was measured using cGMP Direct Chemiluminescent ELISA Kit (Arbor Assays); for both, a CLARIOstar PLUS (BMG Labtech) Microplate Reader was used.

2.6 | Western blot analysis

Twenty transgenic adult animals were transferred into 20-μl M9 buffer and subjected to three freeze–thaw cycles using liquid nitrogen. Subsequently, 4-μl 4× SDS sample buffer was added, followed by boiling (10 min), incubation on ice (5 min), and loading onto a 12% SDS polyacrylamide gel. Subsequently, separated proteins were transferred onto a polyvinylidene fluoride (PVDF) membrane (Roth, Germany), incubated with blocking buffer containing Tris-buffered saline with Tween20 (TBS-T) (20-mM Tris, 0.15-M NaCl, 0.05% Tween20) plus 5% milk powder for 1 h at room temperature. Next, the membrane was incubated with anti-α-tubulin antibody (mouse IgG, 1:50; Piperno and Fuller Cat# 4A1, RRID:AB_2732839) in blocking buffer, washed three times with TBS-T, incubated with anti-mouse IgG secondary antibody conjugated with HRP (1:100; Thermo Fisher Scientific Cat# 32430, RRID:AB_1185566) for 1 h at room temperature in blocking buffer. After three washing steps in TBS-T, detection was performed using GE Healthcare Amersham™ ECL Prime Western-Blot-Detection Reagent (Cytivia, USA) on a ChemoCam ECL & Fluor Blot Imager (Intas Science Imaging, Germany). Afterwards, the membrane was incubated with anti-mCherry (rabbit, 1:10,000; OriGene, Cat# TA150125, RRID:AB_2890005) in blocking buffer for 1 h at room temperature. After three washing steps with TBS-T, the membrane was incubated with anti-rabbit-HRP secondary antibody (1:3000, Carl Roth, Cat# 4750, RRID:AB_2890006) in blocking buffer for 1 h at room temperature, washed three times, and detection was performed as described above. For western blot analysis, the Gel Analyzer plugin in ImageJ was used. For calculation of the relative density values, the percent values of each strain were normalized to the percent value of BeCyclOp(A-2x), depicting the lowest α-tubulin content. Finally, the mCherry/α-tubulin ratio was calculated.

2.7 | Data and statistical analysis

Data are shown as mean ± SEM or mean, median, interquartile range, whiskers (1.5 * IQR), and outliers, with n = number of measured animals. Statistical analyses were performed using GraphPad Prism 8 software (GraphPad Prism, RRID:SCR_002798) or Microsoft Excel 2019 (Microsoft Excel, RRID:SCR_016137). Student's t test, one-way or two-way ANOVA followed by Bonferroni correction as post hoc test were conducted, as indicated in the figure legends. P values ≤0.05 were determined as statistically significant. The data and statistical analysis comply with the recommendations on experimental design and analysis in pharmacology (Curtis et al., 2018).

2.8 | Materials

ATR, IBMX and Tween20 were obtained from Sigma-Aldrich (Darmstadt, Germany). MgSO4, SDS, Tris-HCl, KH_2PO4, Na_2HPO4, NaN_3, NaCl, milk powder, PVDF membrane and the anti-rabbit-HRP secondary antibody were supplied by Roth (Karlsruhe, Germany). The E. coli strain OP50-1 was received from the Caenorhabditis Genetics Center (Minnesota, USA). The AlphaScreen cAMP Detection Kit was purchased from PerkinElmer (Waltham, USA). cGMP Direct Chemiluminescent ELISA Kit was obtained from Arbor Assays (Ann Arbor, USA). The anti-α-tubulin antibody was obtained from the Developmental Studies Hybridoma Bank (Iowa City, USA), and the anti-mouse IgG secondary antibody conjugated with HRP was

received from Thermo Fisher Scientific (Waltham, USA). The GE Healthcare Amersham™ ECL Prime Western-Blot-Detection Reagent was obtained from Cytivia, (Marlborough, USA), and the anti-mCherry antibody was purchased from OriGene (Rockville, USA).

2.9 | Nomenclature of targets and ligands

Key protein targets and ligands in this article are hyperlinked to corresponding entries in the IUPHAR/BPS Guide to PHARMACOLOGY (http://www.guidetopharmacology.org) and are permanently archived in the Concise Guide to PHARMACOLOGY 2019/20 (Alexander, Fabbro et al., 2019; Alexander, Mathie et al., 2019).

3 | RESULTS

3.1 | Two-component optogenetic systems for cGMP generation and depolarization comprising CyclOps or bPGC and the TAX-2/-4 CNG channel

We wanted to expand the optogenetic toolkit for cGMP generation in *C. elegans*. The previously established BeCyclOp enabled the generation of a very high amount of cGMP at a high turnover rate, while the soluble bPGC produced cGMP with low efficiency and slow kinetics (Gao et al., 2015; Woldemariam et al., 2019). Thus, we were looking for a tool with features in between those of BeCyclOp and bPGC, and hence generated or tested different GCs or AC mutants and compared them. To this end, we expressed the proteins in BWM cells, together with the TAX-2/-4 CNG channel, a mostly cGMP-gated, nonselective cation channel (Komatsu et al., 1999; Ramot et al., 2008). TAX-2/-4 activation by cyclic nucleotide monophosphate (cNMP) ($EC_{50}^{cGMP} = 8.4$ μM; $EC_{50}^{cAMP} = 300$ μM, in HEK293 cells; Komatsu et al., 1999) causes muscle depolarization and contraction and thus a macroscopic reduction of the body length that can be measured by video microscopy (Gao et al., 2015; Liewald et al., 2008). Other channels used in this study are as follows (see below): cAMP-gated K^+ channel from *Spirochaeta thermophila* ($EC_{50}^{cAMP} = 3.68$ μM; Brams et al., 2014) and the cGMP-gated K^+-channel BeCNG1 (not activated by cAMP) from *Blastocladiella emersonii* (Avelar et al., 2015). Illumination of animals co-expressing TAX-2/-4 and CaCyclOp (from *Catenaria*) resulted in light-dependent muscle contractions that by amplitude and ON-kinetics fell in between those observed in animals expressing TAX-2/-4; BeCyclOp and TAX-2/-4; bPGC (Figure 1a,b). To more rigorously compare the activities of the GCs, we analysed them at different light levels. Light saturation conditions for each protein were already reached at ≥0.2 $mW{\cdot}mm^{-2}$ (Figure 1c). Furthermore, we determined the expression level of the GCs using western blot analysis (indirectly via mCherry, as each GC transgene also expressed mCherry from a bicistronic mRNA). This indicated the highest expression level for BeCyclOp, and lowest for bPGC. Though we do not know the GC protein expression levels (likely to be lower for the integral membrane proteins), high mRNA levels were in line with more potent optogenetic effects (Figure 1d). Thus, while BeCyclOp is the most potent GC, CaCyclOp is a useful, membrane-bound alternative to bPGC, which is a soluble tool.

3.2 | Implementation and analysis of membrane-bound PACs in cholinergic motor neurons

For the generation of mbPACs, the GC domains of BeCyclOp and CaCyclOp were mutated by distinct changes into AC domains (Linder, 2005; Ryu et al., 2010; Sunahara et al., 1998): BeCyclOp (E497K/C566D), termed "BeCyclOp(A-2x)"; BeCyclOp(E497K/H564D/C566T) = "BeCyclOp(A-3x)"; and CaCyclOp(E497K/C566D) = "CaCyclOp(A-2x)." Previously, we showed that cAMP generation in cholinergic motor neurons via bPAC caused increased neurotransmission and has profound effects on locomotion behaviour (Steuer Costa et al., 2017). Thus, we used this bPAC induced behaviour as a positive control and to compare the effectiveness of the engineered mbPACs. The induced behavioural change could be assessed by the swimming frequency in liquid and by determination of crawling speed and body bending on solid media (Steuer Costa et al., 2017; Weissenberger et al., 2011). Illumination of animals expressing BeCyclOp(A-2x) or bPAC in cholinergic neurons evoked comparably increased swimming cycles and crawling speeds (BeCyclOp(A-2x) appeared even more efficient). However, the effects induced by bPAC decayed faster than those induced by BeCyclOp(A-2x) (Figures 2b,c,e,f and S1A,E,F). In contrast to bPAC, light stimulation of BeCyclOp(A-2x) expressing animals produced no change in their mean bending angles and only a small decrease in body length (Figures 2i,j and S4E,G,H,J). For CaCyclOp(A-2x) and BeCyclOp(A-3x) expressing animals, no light-evoked change in their swimming behaviour was observed (Figures 2b,c and S1B,D,F). With the exception of CaCyclOp(A-2x) expressing animals, all analysed PACs effected decreased basal swimming frequency, compared with the genetic background *lite-1(ce314)* (*lite-1* was used since these animals lack intrinsic photophobicity; Figure S1E,F). Whether this is due to basal (dark) activity of the cyclases or a potential burden due to expression of the foreign protein is unclear, but see below for cAMP measurements in extracts (Figure 3f). Further, BeCyclOp(A-2x) expressing animals exhibited decreased basal crawling speed, independent of the addition of ATR (Figure S4B,D).

To possibly improve expression and/or membrane targeting of the mbPACs, BeCyclOp(A-2x) and CaCyclOp(A-2x) were fused *N*-terminally with yellow fluorescent protein (YFP; Scheib et al., 2018). For YFP-CaCyclOp(A-2x), this improved effects strongly, turning it into a tool as useful as BeCyclOp(A-2x) or YFP-BeCyclOp(A-2x). In both cases, expression of the protein reduced the basal swimming frequency compared to the genetic background (*lite-1(ce314)*), (Figures 2d,g,h,k,l, S5, and S6). This may be due to basal (dark) activity (however, cAMP measurements did not provide indications for this; Figures 3j,k and S7) or could reflect some compromising effect of protein expression on neuronal physiology (e.g., due to evoked ER stress). Light-evoked effects on swimming saturated for YFP-BeCyclOp(A-2x) already at 0.1 $mW{\cdot}mm^{-2}$, while for bPAC, there appeared to be a

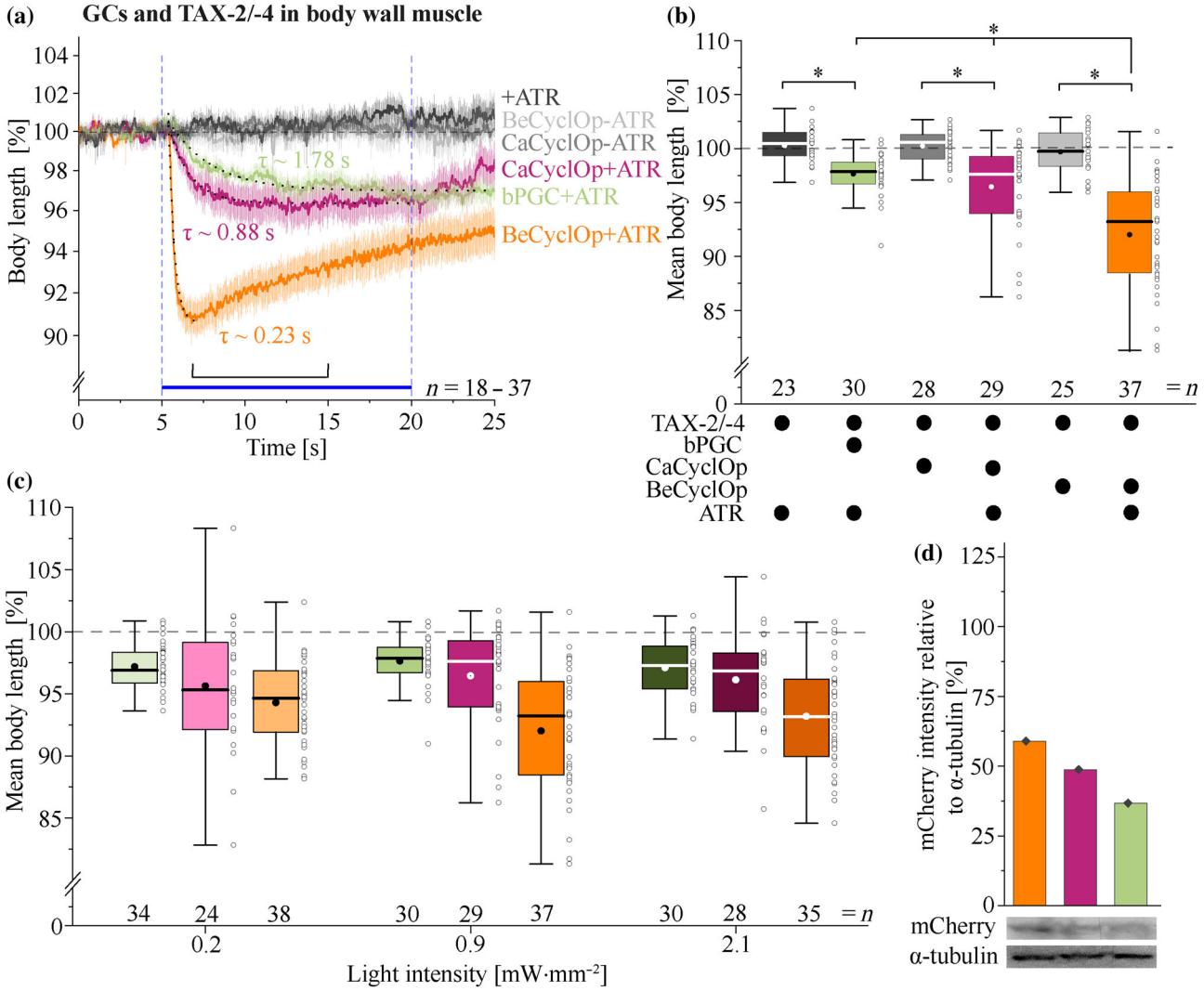

FIGURE 1 Characterization of light activated guanylyl cyclases with respect to CNG-channel mediated muscle contraction. (a) Body length measurements (normalized to the initial length ±SEM) of animals co-expressing the TAX-2/-4 CNG channel and either BeCyclOp, CaCyclOp, or bPGC in body wall muscle cells before, during, and after a 15-s light pulse (0.9 mW·mm^{-2}; 470 nm). Animals were supplemented with (+) or without (−) all-*trans* retinal (ATR). Onset-time constants were determined by fitting as mono-exponential decay (dotted lines). (b) Group analysis for the data in (a) during light stimulation (6.5–15 s). (c) Mean normalized body lengths of animals in (a) during light stimulation at different light intensities, as indicated. (d) Western blot analysis of extracts from transgenic animals expressing the GCs and mCherry from bicistronic pre-mRNAs (including the SL2 trans-splicing sequence). Shown is the mCherry intensity relative to the α-tubulin signal, normalized to the signal of the strain expressing BeCyclOp(A-2x) (Figure 3i) ($N = 1$ sample of $n = 20$ animals each). In (b) and (c), the interquartile range (IQR), median (—), mean values (●), individual measurements (○), and whiskers (1.5 * IQR) are shown. n = number of animals. Blue bar indicates period of illumination. $^{*}P < 0.05$, significantly different as indicated; one-way ANOVA with Bonferroni correction

maximum at 0.2 mW·mm^{-2}, that dropped again at 0.4 mW·mm^{-2}, possibly due to strong body bending counteracting swimming speed (Figure S2A–D). We also determined expression levels of the YFP-CyclOps and bPAC using fluorescence microscopy, depicting much lower levels for the mbPACs (Figure 2m–p). Our analyses show differences in the triggered behavioural output (crawling speed, swimming cycles, body contraction evoked by stimulation of BWMs) and the expression level between the soluble bPAC and the engineered mbPACs: given the lower expression level and higher light sensitivity, BeCyclOp(A-2x); YFP-BeCyclOp(A-2x), and YFP-CaCyclOp(A-2x) are as efficient or even more powerful as the soluble bPAC. This may have to do with the generation of cAMP in vicinity to the membrane, rather than in the cytosol. The details in the parameters of their action that we determined here may enable choosing one tool over another for specific applications (Figure 8, Tables S2 and S3).

3.3 | Evaluating cGMP or cAMP production by membrane-bound PACs

The behavioural analysis of animals expressing mbPACs provided a strong indication that these tools indeed generated cAMP. However,

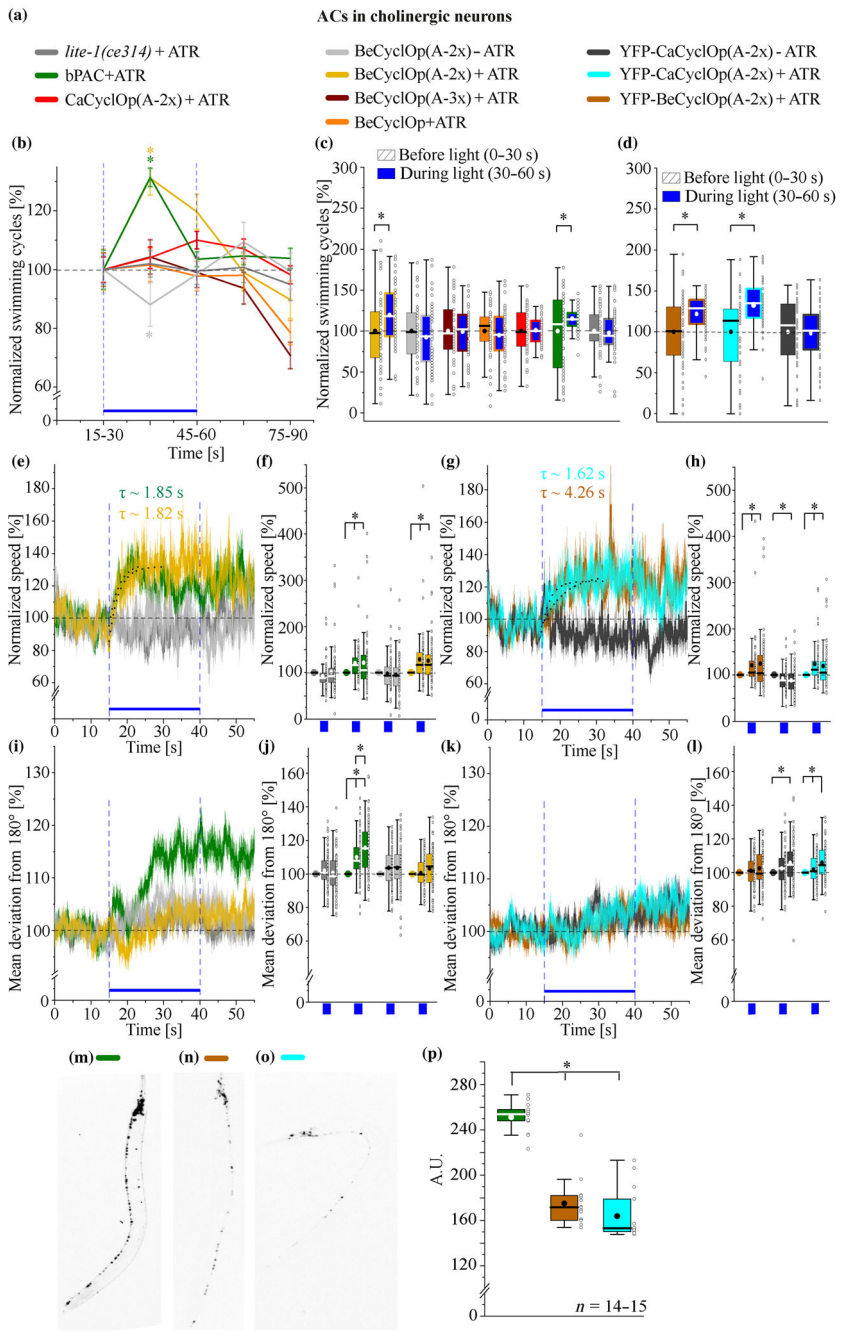

FIGURE 2 Characterizing membrane-bound photoactivatable adenylyl cyclases in cholinergic motor neurons via induced effects on locomotion. (a) Colour code for the analysed strains in (b)–(p). (b) Normalized swimming cycles (±SEM) of animals expressing bPAC, BeCyclOp(A-2x), BeCyclOp(A-3x), wild type BeCyclOp, or CaCyclOp(A-2x) in cholinergic motor neurons of *Caenorhabditis elegans*, in the genetic background *lite-1(ce314)*, during and after a 30-s light pulse (0.2 mW·mm^{-2}; 470 nm). The swimming cycles are normalized to the mean swimming frequency 15 s before light application (n = 40–50). (c,d) Mean swimming cycles 30 s before and 30 s during illumination of the animals in (b) (c, n = 40–50) and of animals expressing YFP-BeCyclOp(A-2x) or YFP-CaCyclOp (A-2x) (d, n = 39–52), normalized to the mean swimming frequency 30 s before the light stimulus. (e,g) Time course of the speed (normalized to the first 15 s without light; ±SEM) of the genetic background *lite-1(ce314)* and animals expressing bPAC or BeCyclOp(A-2x) (e), or YFP-BeCyclOp(A-2x) or YFP-CaCyclOp(A-2x) (g) (e: n = 47–72; g: n = 47–64). (f,g) Mean normalized speed of the time periods before (0–15 s), during (15–40 s; blue bar), and after (40–55 s) illumination (0.2 mW·mm^{-2}; 470 nm) (f: n = 66–72; h: n = 58–61). (i,k) Normalized bending angles (±SEM) of the animals in (e) and (g) (i: n = 47–72; k: n = 47–64). (j,l) Mean normalized bending angles before, during, and after light (j: n = 66–72; l: n = 58–61). Fluorescence images of animals expressing bPAC-YFP (m), YFP-BeCyclOp (A-2x) or YFP-CaCyclOp(A-2x) in cholinergic neurons. (p) Mean fluorescence intensities of animals in (m)–(o). n = number of animals. The blue bars indicate the period of illumination. Shown in (c), (d), (f), (h), (j), (l), and (p) are the interquartile range (IQR), median (—), mean values (●), individual measurements (○), and whiskers (1.5 * IQR). $^{*}P < 0.05$, significantly different as indicated; one-way ANOVA and Student's t test (b,c,d) or one-way ANOVA with Bonferroni correction (e–l,p)

the actual extent of the specificity change and the potential of remaining cGMP production could not be analysed accurately this way. Thus, to further evaluate the mbPACs for their yield of optogenetic cNMP production, they were co-expressed with the TAX-2/-4 CNG channel in BWM cells of *C. elegans*. This channel is mostly specific for cGMP, although it can also be activated by cAMP, with 200-fold lower sensitivity. We then used body length measurements (following photostimulation) to assess the respective mbPACs for possibly remaining cGMP production (that would efficiently activate the CNG channel and evoke body contraction), as well as induced cAMP production (this would evoke contraction if considerable amounts of cAMP would be generated, or a mixture of cGMP and cAMP) (Gao et al., 2015). With exception of CaCyclOp(A-2x), that was ineffective, light stimulation (2 s, 535 nm) of all mbPACs evoked similar overall body contraction (Figure 3b,c). Importantly, none of the mbPACs induced contractions as effectively as BeCyclOp, in line with the largely reduced activation of the CNG channel by cAMP. Slight differences in the light-triggered behavioural changes induced by the mbPACs are present in the time course, while the effect induced by TAX-2/-4; BeCyclOp(A-2x) expressing animals decayed much more slowly (Figure 3b). Interestingly, in contrast to CaCyclOp(A-2x), YFP-CaCyclOp(A-2x) could mediate a light-triggered body contraction, whereas in comparison to BeCyclOp(A-2x), YFP-BeCyclOp(A-2x) exhibited a faster decay of the evoked effect (Figure 3b). To further

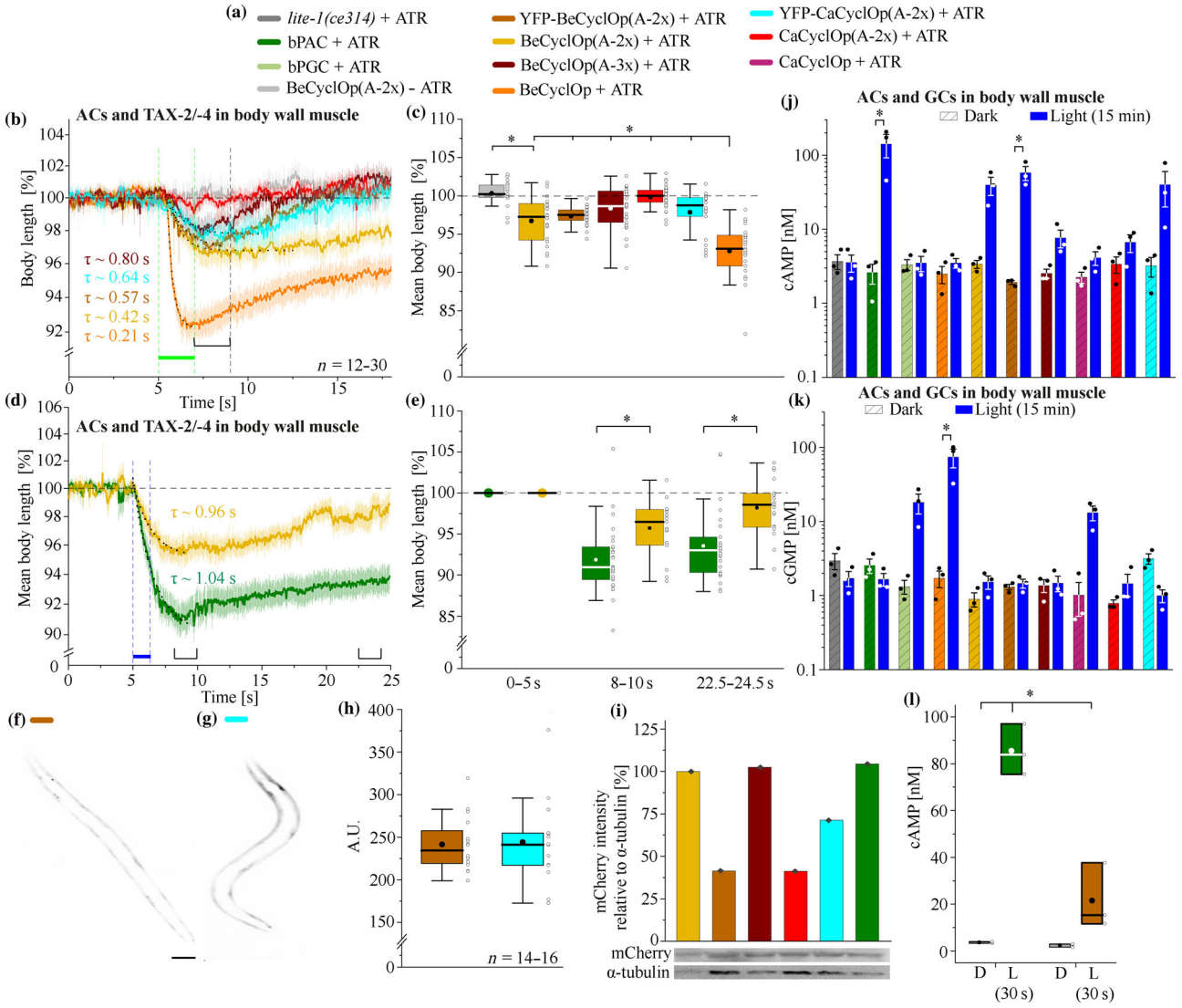

FIGURE 3 mbPACs and the TAX-2/-4 CNG channel in body wall muscle cells show different efficiency and kinetics in cNMP generation. (a) Colour code for the investigated strains in (b)–(e) (all strains express the TAX-2/-4 CNG channel). (b) Body lengths (±SEM) of TAX-2/-4-expressing animals co-expressing BeCyclOp(A-2x), YFP-BeCyclOp(A-2x), BeCyclOp(A-3x), wild type BeCyclOp, CaCyclOp(A-2x), or YFP-CaCyclOp(A-2x) in body wall muscle cells, before, and after a 2-s light pulse (0.9 mW·mm^{-2}; 535 nm). Time constants were calculated by nonlinear fitting for monoexponential decay of the body lengths (dotted lines). (c) Body length reductions after light application (7–9 s), triggered by optogenetic cNMP generation and TAX-2/-4 activation ($n = 17–27$). (d) Body length measurements (±SEM) of animals, co-expressing TAX-2/-4 and either BeCyclOp(A-2x) or bPAC before and after a 2-s light pulse (0.9 mW·mm^{-2}; 470 nm) ($n = 16–27$). (e) Mean normalized body lengths for the time periods before (0–5 s), during (8–10 s), and after (22.5–24.5 s) light stimulation ($n = 19–28$). Fluorescence images of animals expressing YFP-BeCyclOp(A-2x) (f) or YFP-CaCyclOp(A-2x) (g). (h) Mean fluorescence intensities of animals in (f) and (g). (i) Western blot analysis of animals expressing the respective adenylyl cyclase and mCherry, from a bicistronic mRNA, resulting in the translation of two separated proteins. Shown is the mCherry intensity relative to the α-tubulin signal, normalized to the signal of the strain BeCyclOp(A-2x) ($N = 1$ replicate of $n = 20$ animals). (j,k) Quantification of cAMP (j) and cGMP (k) levels using *Caenorhabditis elegans* extracts. Animals expressing bPAC, bPGC, BeCyclOp, BeCyclOp(A-2x), YFP-BeCyclOp, BeCyclOp(A-3x), CaCyclOp, CaCyclOp(A-2x), or YFP-CaCyclOp(A-2x) were illuminated with blue light (0.5 mW·mm^{-2}; 470 nm, 15 min) or incubated with red filtered transmission light (675 nm; 15 min) as dark condition. Data shown are the mean values (±SEM) including the individual measured values (●). $n = 3$ samples of 60 animals each. (l) Quantification of cAMP levels of animals expressing bPAC or YFP-BeCyclOp(A-2x), illuminated for 30 s with blue light (light = L) (0.5 mW·mm^{-2}; 470 nm) or with red filtered transmission light (675 nm) (dark = D). $N = 3$ replicates of $n = 60$ animals each. In (c), (e), (h), and (l), the interquartile range (IQR), median (—), mean values (●), individual measurements (○), and whiskers (1.5 * IQR) are shown. The green and blue bar indicate the period of illumination. $^{*}P < 0.05$, significantly different as indicated; one-way ANOVA with Bonferroni correction (b-e) or two-way ANOVA with Bonferroni correction (j–l)

classify the cNMP production generated by BeCyclOp(A-2x), we compared changes in the body lengths due to light application (2 s, 470 nm) between TAX-2/-4; BeCyclOp(A-2x) and TAX-2/-4; bPAC expressing animals. Here, bPAC induced a stronger body contraction, indicating higher overall cAMP production than mbPAC (Figure 3d,e). Body contraction evoked by bPAC, via TAX-2/-4 channels showed

light saturation at 0.2 mW·mm^{-2} (Figure S2E,F), thus much below the light intensity used for the comparison of the tools described above. We note that some BeCyclOp(A-2x) expressing animals had altered morphology, that is, shortened and wider body, for unknown reasons. Such animals were excluded from our analyses.

The expression levels of the respective PACs were determined by western blot analysis and fluorescence microscopy. The results showed the highest expression levels for BeCyclOp(A-2x), BeCyclOp(A-3x), and bPAC, whereas YFP-CyclOp(A-2x)s showed about half or intermediate expression levels (Figure 3f–i).

Because both cGMP and cAMP can activate the TAX-2/-4 CNG channel, leaving some ambiguity in the interpretation of the above results, we wanted to use a more defined assay probing for cAMP and cGMP production and specificity. We thus employed in vitro assays for cAMP and cGMP quantification, measuring the cNMP content of a fixed number of animals (i.e., their entire body) after 15 min of illumination. Here, for BeCyclOp(A-2x), YFP-BeCyclOp(A-2x), and YFP-CaCyclOp(A-2x), we could determine a high level of cAMP produced in transgenic *C. elegans* tissue, though not reaching the same extent as the soluble bPAC (bPAC produced ca. 2.5× more cAMP than YFP-BeCyclOp(A-2x); dark activity could not be determined with this assay, as cAMP levels in dark were as in non-transgenic controls). Importantly, none of the mbPACs showed any measurable cGMP production (Figures 3f,g and S7). To measure optogenetic cAMP generation at conditions that match the behavioural experiments, we stimulated the animals with blue light (470 nm) for only 30 s. Here, the cAMP level for bPAC was about fourfold higher compared to the mbPAC (Figure 3l). For GCs, cGMP production was highest for BeCyclOp, while bPGC and CaCyclOp were comparable, generating approximately 4.5 times less cGMP than BeCyclOp. In sum, BeCyclOp proved to be the most potent mbPGC optogenetic tool, while the novel engineered optogenetic cAMP tools produce (and accumulate) cAMP at high levels in vivo, with high specificity. The effective induction of behaviour by the engineered mbPACs compared to bPAC, despite much lower cAMP generation at brief illumination periods, emphasizes the higher effectivity of the mbPACs in generating membrane proximal cAMP.

3.4 | Combining BeCyclOp and the cGMP-gated K$^+$-channel BeCNG1 for K$^+$-based cell hyperpolarization

Recently, the cGMP-gated K$^+$-channel BeCNG1 (not activated by cAMP) was found in the genome of the aquatic fungus *Blastocladiella emersonii* and characterized as the effector protein downstream of BeCyclOp, participating in the phototactic response of the zoospore (Avelar et al., 2015). We wanted to adopt this mechanism to achieve optogenetic hyperpolarization using K$^+$-conductance, for which only few examples have been demonstrated so far. We thus co-expressed BeCyclOp and the BeCNG1 channel in BWM cells (Figure 4a,b) to obtain a two-component optogenetic system for the manipulation of K$^+$ currents. Optogenetic cGMP production should activate the BeCNG1 channel, thus triggering muscle hyperpolarization and body elongation (Gao et al., 2015; Liewald et al., 2008). BeCNG1-YFP showed a clustered appearance along the muscle membrane (Figure 4a). Illumination of animals co-expressing BeCNG1 and BeCyclOp, supplemented with ATR, evoked a slightly increased body length within ∼3 s, which remained at this level even after turning light off (Figure 4c,d). No effects were observed in control animals cultivated without ATR. As we showed earlier, animals expressing only BeCyclOp do not exhibit changes in body length (Gao et al., 2015). In conclusion, BeCyclOp and BeCNG1 achieved moderate but long-lasting optogenetic hyperpolarization of BWM cells of *C. elegans*.

3.5 | Implementation of the cAMP-gated K$^+$-channel SthK and bPAC in BWM cells

Previously, a two-component optogenetic silencing system, consisting of bPAC and the cAMP-gated SthK channel from *Spirochaeta thermophila* ($EC_{50}^{cAMP} = 3.68$ µM, in *Xenopus* oocytes; Brams et al., 2014), was used to manipulate K$^+$ currents in various model organisms (Beck et al., 2018; Bernal Sierra et al., 2018). To analyse the functionality of this system in *C. elegans*, we co-expressed the SthK channel and bPAC in BWM cells (Figure 5a) and performed behavioural experiments, that is, swimming and body length measurements. Muscle hyperpolarization decreases swimming frequency and increases body length (Zhang et al., 2007). Expressing the SthK channel alone reduced the basal swimming frequency, compared with the genetic background *lite-1(ce314)*, likely due to intrinsic cAMP, and this was further decreased by co-expression with bPAC, even in the dark, arguing for effects of the known dark activity of bPAC (Figure 5b). Illumination of SthK; bPAC expressing animals, however, caused a complete arrest of their swimming behaviour (Figure 5b). In body length measurements, light stimulation caused long-lasting elongation of approximately 4%, that is, comparable to other strong hyperpolarizers like GtACR2 or Arch (Bergs et al., 2018; Husson, Liewald, et al., 2012), within ∼1 s (Figure 5c,d), which lasted up to 10 min (Figure S8), possibly, as *C. elegans* BWM expresses no or only low levels of phosphodiesterases. In conclusion, bPAC and SthK evoked light dependent, robust, long-term muscle hyperpolarization. However, SthK is so sensitive that intrinsic cAMP levels already suffice for its activation.

3.6 | mbPACs enable more precise control of the SthK channel for inhibition in BWM cells

Because the SthK channel is very sensitive and activated by very low levels of cAMP, and bPAC produces very high amounts of cAMP and exhibits dark activity, we combined SthK with the engineered variants of the cyclase rhodopsins. These should have no dark activity and produce lower amounts of cAMP, as shown in our in vitro assays (Figures 3f,g and S7A,B). We co-expressed the SthK channel with the CyclOp PACs (mbPACs) in BWM cells and investigated their

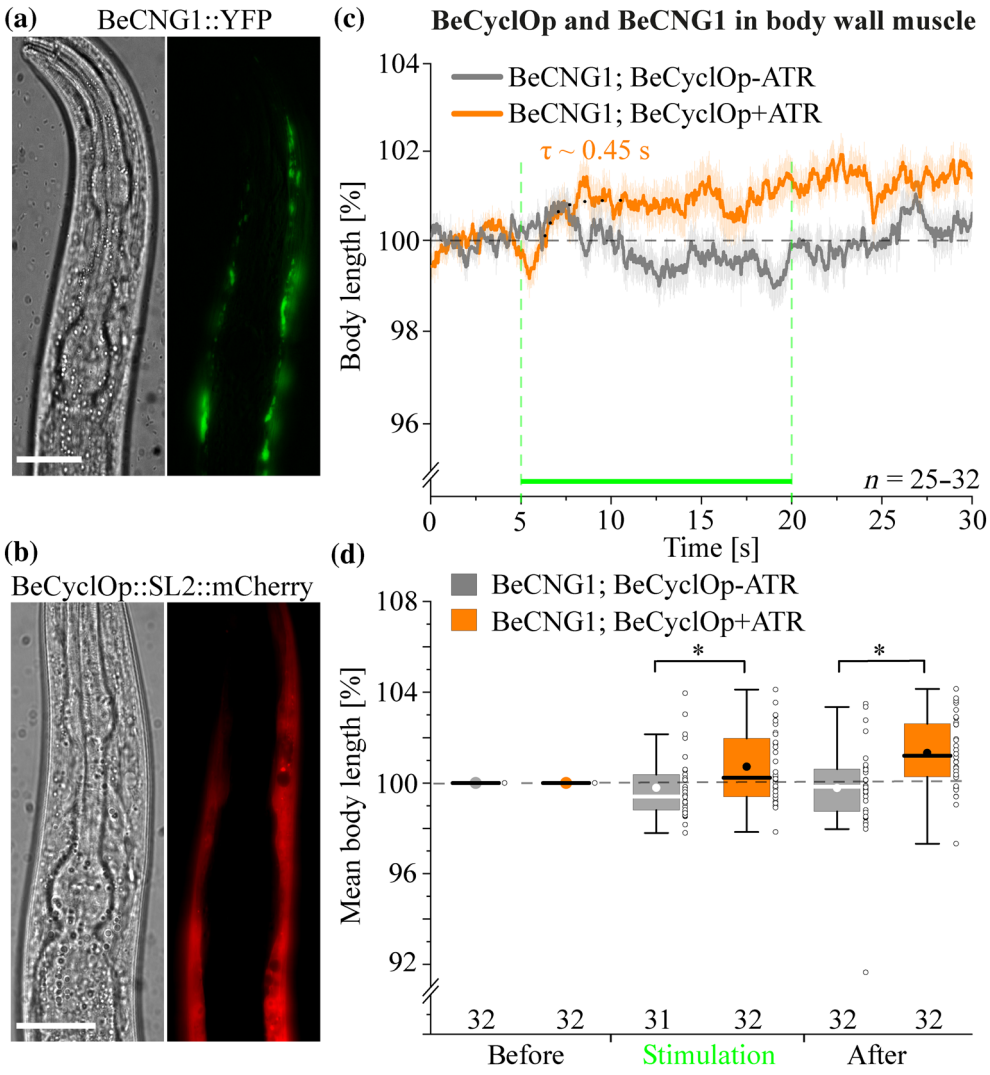

FIGURE 4 BeCyclOp and the cGMP-gated BeCNG1 K^+-channel trigger muscle hyperpolarization. Co-expression of BeCNG1-YFP (a) and BeCyclOp::SL2::mCherry (b) in BWMs of *Caenorhabditis elegans*. Scale bar, 50 µm. (c) Body length measurements (±SEM) of animals co-expressing BeCNG1 and BeCyclOp, supplemented with (+) or without (−) ATR before, during and after a 15-s light pulse (0.9 mW·mm^{-2}; 535 nm). Onset-time constant was determined by fitting as mono-exponential growth (dotted line). (d) Group data, mean normalized body lengths for the time periods before (0–5 s), during (5–20 s), and after (20–30 s) light application. Displayed are the interquartile range (IQR), median (—), mean values (●), individual measurements (○), and whiskers (1.5 * IQR). *n* = number of animals. The green bar indicates the period of illumination. $^*P < 0.05$, significantly different as indicated; one-way ANOVA with Bonferroni correction

hyperpolarizing potential and light control using swimming assays and body length measurements. First, we investigated the parental cyclase, BeCyclOp, in combination with SthK. Interestingly, illumination of animals co-expressing SthK and wild type BeCyclOp increased the swimming cycles and decreased the body length, possibly because cGMP acts an antagonist (Kesters et al., 2015), or agonist with low efficacy (Schmidpeter et al., 2018) (Figure 6a–c).

Next, we tested the mbPAC variants, as these produce lower amounts of cAMP and could thus lead to preferable outcomes in the evoked effects on muscle hyperpolarization. Animals co-expressing SthK and BeCyclOp(A-2x) showed a high variability in their swimming frequency, independent of the addition of ATR, which was not observed for SthK; BeCyclOp(A-3x) animals (Figure 6a). In contrast to this, SthK; CaCyclOp(A-2x) expressing animals exhibited a decreased basal swimming frequency in comparison to SthK expressing animals (Figure 6a). Illumination of the SthK; BeCyclOp(A-2x) and (A-3x) variant expressing animals reduced the swimming cycles, although it did not trigger a complete arrest (Figure 6a). Also, light stimulation of these animals increased the body length (Figure 6b,c). Whereas for SthK; BeCyclOp(A-3x) animals, the evoked hyperpolarization reached a higher level and decayed a few seconds after turning off the light; it remained constant for SthK; BeCyclOp(A-2x) animals (Figure 6b). For SthK; CaCyclOp(A-2x) animals, light application slightly decreased the swimming rate and had no influence on their body length (Figure 6a–c). Overall, the combination of SthK and BeCyclOp(A-3x) appears to be the most favourable for K^+-based inhibition: Adding BeCyclOp(A-3x) had no influence on the basal swimming rate of animals expressing SthK, and light triggered a strong inhibition and body elongation. As light did not trigger a complete arrest of swimming, we tried to improve this by increasing the expression level of BeCyclOp(A-3x). However, this reduced the basal swimming cycles independent of ATR supplementation (Figure S9); thus, the expression levels need to be titrated for optimal performance.

3.7 | PACs and the SthK channel in cholinergic neurons

Last, we assessed the SthK and PAC systems for their ability to hyperpolarize *C. elegans* cholinergic neurons, by analysing swimming behaviour. As observed in muscle, expression of the SthK channel

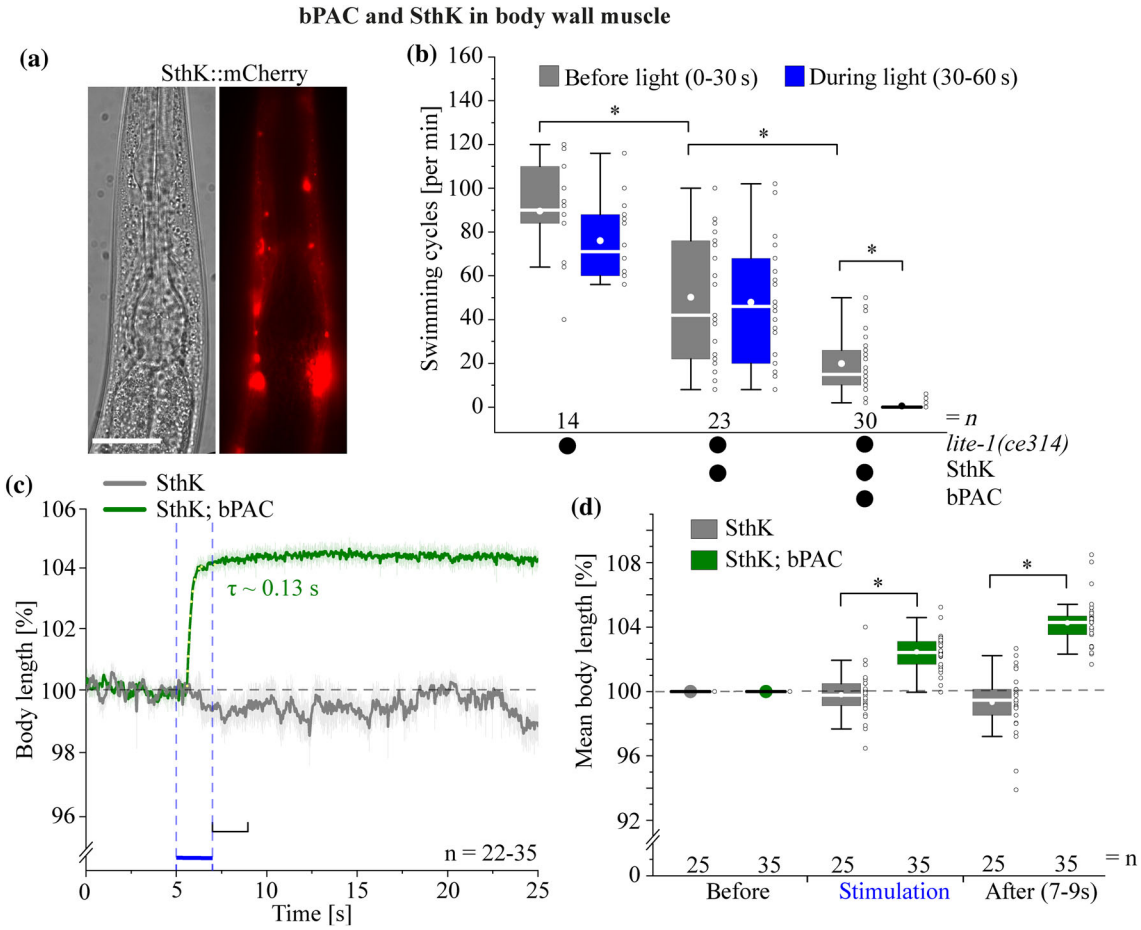

FIGURE 5 Establishment of the SthK channel and bPAC as a two-component optogenetic system for the manipulation of K^+ currents in BWM cells. (a) Fluorescence micrograph (right) and DIC brightfield image (left) of the head of an animal expressing SthK-mCherry in BWM cells (anterior is up). Scale bar, 50 µm. (b) Swimming behaviour of animals expressing either SthK alone or co-expressing SthK and bPAC, as well as the genetic background *lite-1(ce314)*. Swimming cycles (±SEM) were calculated 30 s before, and 30 s during light stimulation (0.2 mW·mm^{-2}; 470 nm). (c) Body length measurements (±SEM) of animals expressing either SthK alone or co-expressing SthK and bPAC before and after a 2-s light pulse (0.9 mW·mm^{-2}; 470 nm). Onset-time constant was determined by fitting as mono-exponential growth (dotted line). (d) Mean normalized body lengths before (0–5 s), during (5–7 s), and after (7–9 s) illumination. In (b) and (d), the interquartile range (IQR), median (—), mean values (●), individual measurements (○), and whiskers (1.5 * IQR) are shown. *n* = number of animals. The blue bar indicates the period of illumination. $^*P < 0.05$, significantly different as indicated; one-way ANOVA and Student's *t* test (b) and one-way ANOVA with Bonferroni correction (d)

decreased the basal swimming rate in the genetic background *lite-1 (ce314)* and in wild-type animals (as expected, because these neurons use cAMP for intrinsic signalling to regulate transmitter output and neuropeptide release; Steuer Costa et al., 2017), which was further reduced by co-expression with bPAC and the likely increased cAMP levels due to its dark activity (Figure 7b). Illumination of these animals depressed the swimming frequency to nearly complete arrest (Figure 7b,c). This effect was long lasting, and the swimming rate increased again after 90–150 s following the end of the illumination (Figure 7c). As the reduction of swimming rate by SthK and bPAC co-expression was already substantial in the dark, this combination of tools appears of limited use in *C. elegans*, unless one wants to achieve permanent K^+-based inhibition. Thus, we investigated if co-expression of SthK with BeCyclOp(A-2x) or BeCyclOp(A-3x) would be an alternative for this cell type. Using the same expression level of SthK as used before, no viable mbPAC transgenes were obtained. Consequently, we reduced the expression level of SthK. Still, all transgenes decreased basal swimming rates (Figure 7d), though not as much as for SthK expressed at higher levels. Light stimulation of these animals evoked a further, robust decrease in swimming frequency, which increased again after turning off the light (Figure 7d,e). In an attempt to optimize the system, we combined YFP-BeCyclOp(A-2x) with low levels of SthK. This restored the normal basal swimming rate but no light-dependent inhibition was detectable (Figure 7f,g). Possibly, the relative expression might be further titrated to achieve an optimum. The best results were obtained with BeCyclOp(A-2x) with low SthK expression. To summarise, SthK in combination with bPAC or the BeCyclOp PACs are able to hyperpolarize cholinergic neurons in *C. elegans*. However, they also affect the physiology, most probably the resting potential of the neurons.

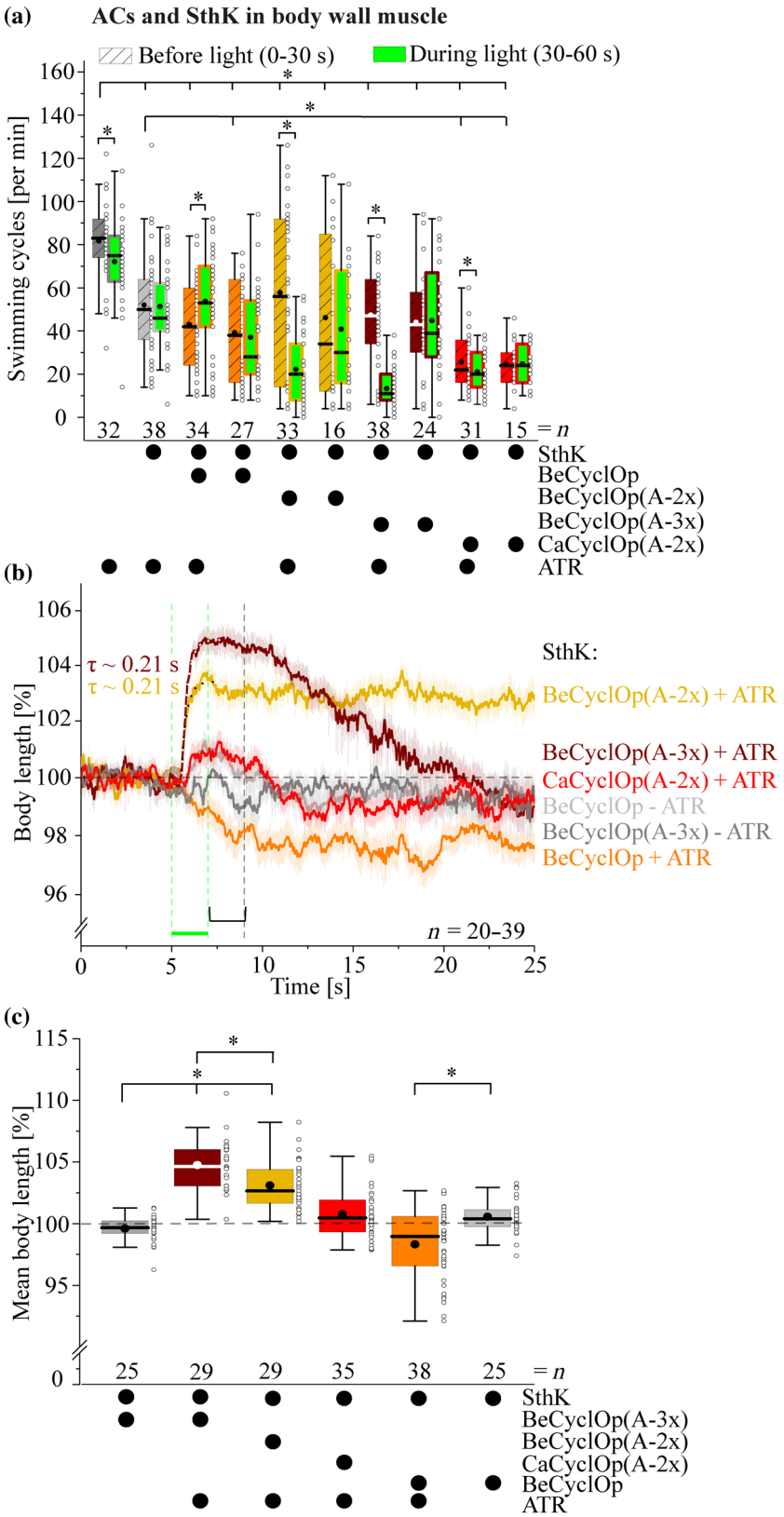

FIGURE 6 Membrane-bound PACs and SthK as tools for the manipulation of K^+ currents. (a) Swimming behaviour of animals expressing the SthK channel alone or with wild type BeCyclOp, BeCyclOp(A-2x), BeCyclOp(A-3x), or CaCyclOp(A-2x), respectively, in the genetic background *lite-1 (ce314)*. Swimming cycles (±SEM) were calculated 30 s before and 30 s during light application (1 mW·mm^{-2}; 535 nm). (b) Body lengths (±SEM) of animals co-expressing SthK and wild type BeCyclOp, BeCyclOp(A-2x), BeCyclOp(A-3x), or CaCyclOp(A-2x) before and after a 2-s light pulse (0.9 mW·mm^{-2}; 535 nm). Onset-time constants were determined by fitting as mono-exponential growth (dotted line). (c) Mean normalized body lengths of the animals shown in (b) after light stimulation (7–9 s). Shown in (a) and (c) are the interquartile range (IQR), median (—), mean values (●), individual n values (○), and whiskers (1.5 * IQR). *n* = number of animals. The green bar indicates the period of illumination. $^*P < 0.05$, significantly different as indicated; one-way ANOVA and Student's *t* test (a) and one-way ANOVA with Bonferroni correction (c)

4 | DISCUSSION

In this study, we present a comprehensive optogenetic toolbox for cGMP and cAMP manipulation in excitable cells of *C. elegans*, as well as a combination with depolarizing and K^+-specific hyperpolarizing CNG channels for two-component optogenetics. We analysed the *C. anguillulae* CyclOp for its efficiency in optogenetic cGMP production and characterized engineered adenylyl cyclases, emerging by

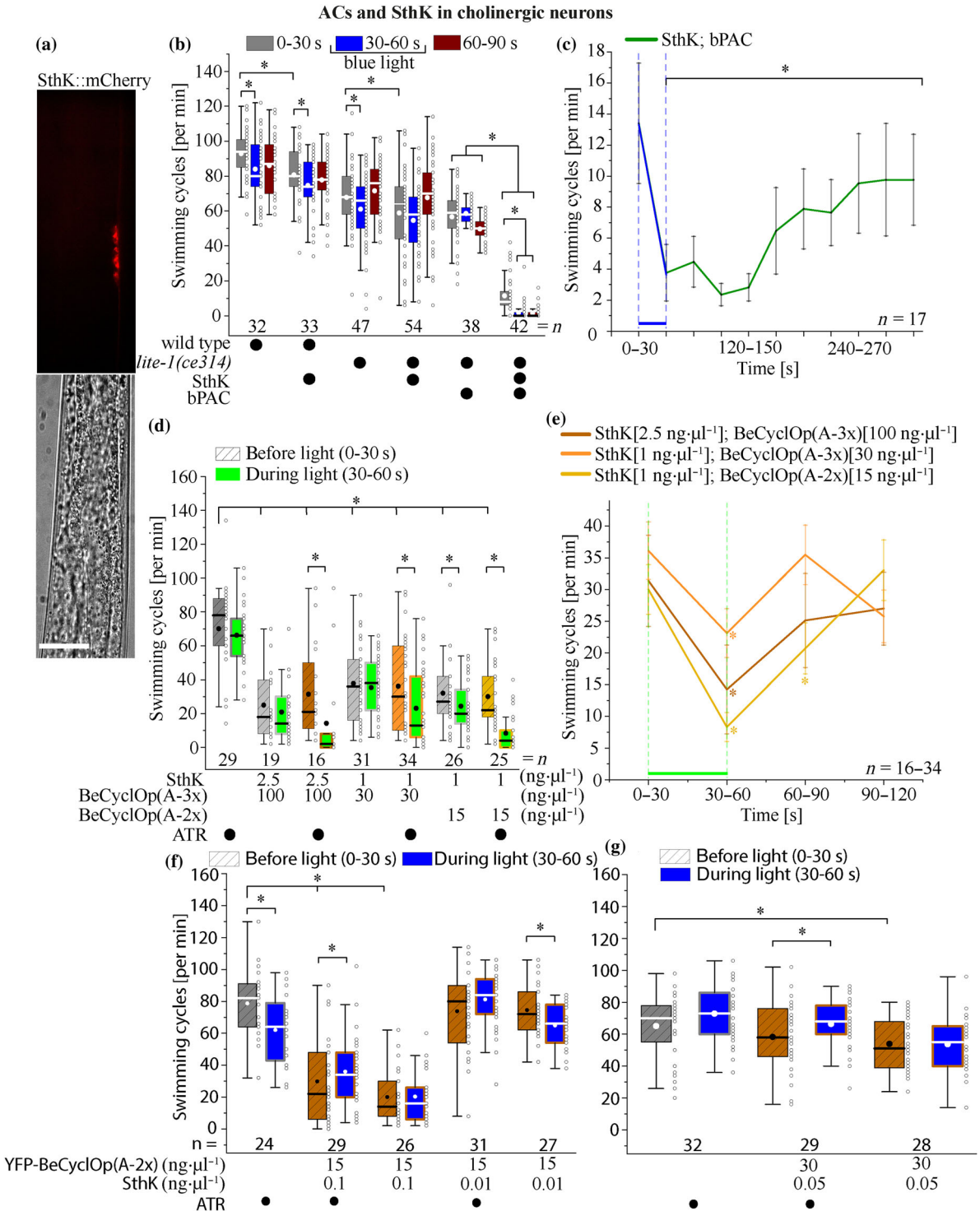

FIGURE 7 Application of bPAC or mbPACs and the SthK channel for hyperpolarization of cholinergic neurons. (a) Expression of SthK-mCherry in cholinergic neurons of *Caenorhabditis elegans*. Scale bar is 50 µm. (b) Swimming behaviour (±SEM) analysis of animals expressing SthK, bPAC, or co-expressing SthK and bPAC, the genetic background *lite-1(ce314)* and wild-type animals, 30 s before and 30 s after a 30-s light pulse (0.4 mW·mm^{-2}; 470 nm). (c) Swimming cycles (±SEM) of animals co-expressing SthK and bPAC 30 s before and 270 s after 30-s light application (0.4 mW·mm^{-2}; 470 nm). (d,f,g) Swimming frequency (±SEM) of animals co-expressing the SthK channel and BeCyclOp(A-3x) or BeCyclOp(A-2x) (D) or YFP-BeCyclOp(A-2x) (f,g) in the genetic background *lite-1(ce314)*, 30 s before and during a 30-s light pulse (1.35 mW·mm^{-2}; 535 nm (d), 0.4 mW·mm^{-2}; 470 nm (f,g). Strains were generated using different amounts of plasmid DNA (indicated by ng·µl^{-1}). (e) Swimming behaviour (±SEM) analysis of animals in (d), 30 s before and 60 s after a 30-s light pulse (1.35 mW·mm^{-2}; 535 nm). In (b), (d), (f), and (g), the interquartile range (IQR), median (—), mean values (●), individual measurements (○), and whiskers (1.5 * IQR) are shown. *n* = number of animals. The green and blue bars indicate the period of illumination. $^{*}P < 0.05$, significantly different as indicated; one-way ANOVA and Student's *t* test (b,d,e) and paired Student's *t* test (c)

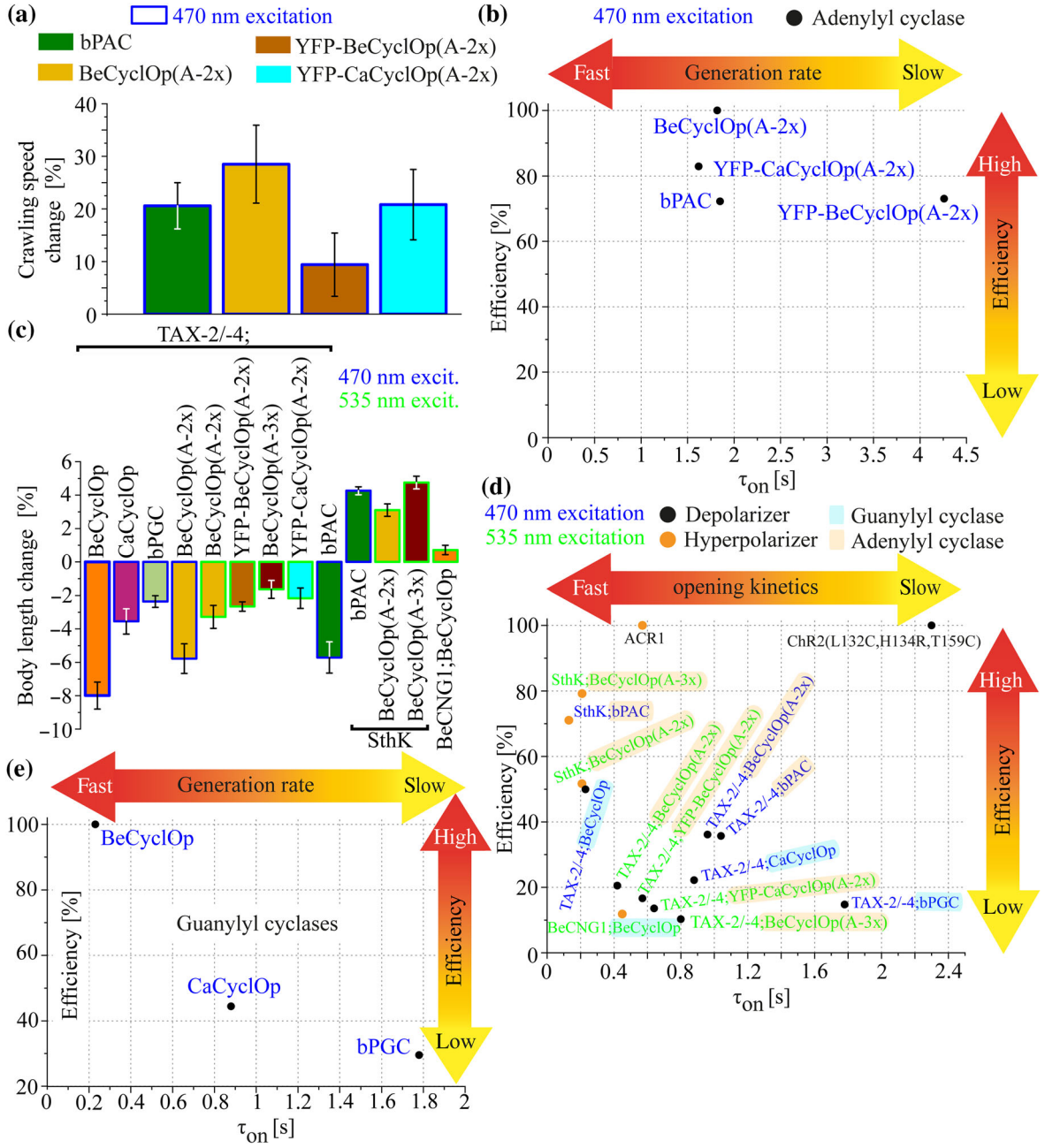

FIGURE 8 Evaluation of guanylyl and adenylyl cyclases, as well as depolarizing and hyperpolarizing two-component optogenetic tools characterized in this paper. (a) Changes in crawling speed triggered by adenylyl cyclases. Data shown are the mean normalized speed (±SEM) relative to the initial crawling speed of the animal. (b) Scheme of photoactivatable adenylyl cyclases expressed in cholinergic neurons, classified by the time course of evoked behavioural changes, as a proxy for cAMP generation rate (τ) and efficiency. The efficiency was calculated as follows: comparison of crawling speed changes, induced by the respective tool (0.2 mW·mm^{-2}; 470 nm), relative to the maximum crawling speed increase. The best performing tool (BeCyclOp(A-2x)) was arbitrarily set to 100% efficiency. (c) Body length changes evoked by depolarizing and hyperpolarizing combinations of cyclases and CNG channels, as indicated. Shown is the mean normalized body length (±SEM) relative to the initial body length of the animal. (d) Scheme of optogenetic depolarizer and hyperpolarizer two-component optogenetic tools, as well as ChR2 and ACR1 "benchmarks," expressed in body wall muscle cells, categorized by opening kinetics (τ) and efficiency. The efficiency was estimated as follows: depolarizer (hyperpolarizer)—comparison of body length reduction (increase), evoked by the respective tool (0.9 mW·mm^{-2}; 470 nm; 535 nm) relative to the maximum body length decrease (elongation); 100% efficiency was arbitrarily set for the best performing optogenetic tools in such assays, ChR2(L132C, H134R, T159C) and ACR1 (Bergs et al., 2018). (e) Photoactivatable guanylyl cyclases expressed with the TAX-2/-4 CNG channel in body wall muscle, classified by the time course of evoked behavioural changes, as a proxy for cGMP generation rate (τ) and efficiency. The efficiency was calculated as follows: comparison of body length changes, induced by the respective tool (0.9 mW·mm^{-2}; 470 nm), relative to the initial body length. The best performing tool (BeCyclOp; see panel c) was arbitrarily set as being 100% efficient. It should be kept in mind that the relative placement of the proteins in panels (b), (d), and (f) could be altered by changing expression levels and intensity of light stimulation. Data in this paper provide a guideline on which factors may be altered to fine-tune the activity of the optogenetic tools

conversion of the guanylyl cyclase domains of BeCyclOp and CaCyclOp, for light-induced cAMP generation in *C. elegans*. These tools were combined with different cNMP-gated channels and assessed for their potential to activate or silence BWM cells or cholinergic neurons, highlighting different combinations with different relative expression levels, light saturation properties, levels of activity, kinetics, and long- or short-lasting effects (Figure 8). Thus, researchers can choose the appropriate tool for their specific application, for example, in experiments addressing effects of candidate drugs on a particular behaviour, affected by cyclic nucleotides or membrane potential changes, in cells of the nematode, for example, the pharynx that can serve as a cardiac model (Fischer et al., 2017; Schuler et al., 2015).

Until now, BeCyclOp was the only mbPGC implemented in *C. elegans* (Gao et al., 2015). cGMP generation by BeCyclOp is characterized by a high magnitude reached within a few seconds (Gao et al., 2015; Scheib et al., 2015). Depending on the cell type in which the tool is expressed, application could be accompanied by overactivation of cGMP signalling pathways or by cross-talk to cAMP signalling or NTP utilizing pathways, for example, due to macroscopic depletion of GTP or NTPs via interconverting enzymes, thus interfering with the cellular output or metabolism of the cell. To overcome this problem, we characterized CaCyclOp, which is less efficient than BeCyclOp (Gao et al., 2015), for its applicability in *C. elegans*: CaCyclOp showed lower light inducible cGMP production, slower cGMP production rate, but similarly high substrate specificity, when compared to BeCyclOp. Thus, CaCyclOp enables fine-tuning of cGMP levels, which makes it a beneficial optogenetic tool for future studies of cGMP signalling, comprising mbPGCs for signal transmission. Specific subcellular targeting would allow studies of cGMP signalling closer to physiological conditions, allowing its application in *C. elegans* research areas such as sensory signalling and plasticity or regulation of the dauer arrest (Bargmann & Horvitz, 1991; Birnby et al., 2000; Fielenbach & Antebi, 2008; Schultheis et al., 2011). Our test system, in combination with the possibility of studying subcellular cGMP signalling within a living organism, would further support the development of mbPGCs and their application in higher organisms with a need for spatial and temporal control of cGMP levels, not only through subcellular localization of PDEs (Bock et al., 2020; Houslay, 2010) but also by local photoactivation, thus allowing new insights into cellular processes such as cell growth and survival.

Previously, the existing optogenetic tools for cAMP generation in *C. elegans* were soluble proteins. These did not mimic the physiological conditions under which cAMP is produced by mbACs within microdomains in close vicinity to the PM (Bock et al., 2020; Cooper, 2003; Etzl et al., 2018; Ryu et al., 2014; Steuer Costa et al., 2017; Weissenberger et al., 2011). To generate mbPACs, we used CyclOps and converted them into ACs by specific mutations. Amongst the analysed mbPACs, YFP-CyclOps and BeCyclOp(A-2x) showed the highest amounts of light-triggered cAMP produced over a long incubation period (15 min), though not reaching the levels produced by bPAC, and no obvious residual cGMP generation. At shorter time scales, mbPACs produced considerably less cAMP than bPAC. Also, they were expressed at lower levels. Nonetheless, the cAMP production by these tools evoked more potent activation of motor neurons. Besides the desired enhanced locomotion behaviour, we observed differences between behavioural changes induced by local (YFP-CyclOps; BeCyclOp(A-2x)) and cytosolic (bPAC) cAMP signalling in cholinergic neurons, that is, increased diversity of the behavioural output (bending angles, body length; for speed, mbPACs were slightly more effective than bPAC) and a more rapidly decaying response (swimming and crawling behaviour) for cytosolic cAMP signalling. The latter could be a hint that PDEs do not access cAMP generated in the vicinity of the membrane as readily as the cAMP in the cytosol. Generally, undesired cAMP signalling pathways may be activated by cytosolic cAMP generation, thus triggering changes in the bending angles and body length. In contrast, local (membrane proximal) optogenetic cAMP production may more specifically activate cAMP dependent neurotransmission, that is, increased mobilization and priming/docking of synaptic vesicles (SV) and an increased filling of the SVs with **ACh** (Steuer Costa et al., 2017) and thus an increase in locomotion behaviour.

In contrast to CaCyclOp(A-2x), expression of wild type BeCyclOp, mbPAC variants and bPAC reduced the basal swimming frequency, which could be due to a common "toxicity" of these proteins, or due to cNMP production in the dark. Furthermore, expression of BeCyclOp(A-2x) in cholinergic neurons reduced the basal crawling speed, and in some cases, expression in muscle cells changed the morphology of the animals. These observations are independent of ATR addition, thus indicating (some) constitutive cAMP production by this variant, which was also reported before (Trieu et al., 2017). However, as expression of bPAC in cholinergic neurons reduced the basal swimming frequency too, and the YFP-CyclOp variants showed the highest tolerability in these neurons, they constitute the preferred optogenetic tools and may facilitate studies, for example, in neuropeptidergic signalling, memory formation, or cell growth. Activation of BeCyclOp(A-3x) in cholinergic neurons evoked no obvious behavioural changes; however, a light-dependent increase in cAMP by expression in muscle cells (co-expressed with TAX-2/-4 or SthK) could be detected. Due to the generation of low amounts of cAMP, this variant could be of interest for further studies of cAMP signalling (Rost et al., 2017).

Generation of second messengers is accompanied by amplification of the primary signal, making combinations of photoactivated nucleotide cyclases (PNCs) and CNG channels useful tools due to a reduced need for light. Aiming at multicomponent systems for the depolarization of excitable cells, we combined the TAX-2/-4 CNG channel with PNCs. In this context, none of the analysed systems were able to induce comparably high depolarization effects as the previously implemented TAX-2/4; BeCyclOp system in regard of the magnitude (Gao et al., 2015); however, in contrast to this system, no desensitization was observed for TAX-2/-4 combined with BeCyclOp(A-2x), CaCyclOp, or bPGC. Yet, these systems require the expression of three genes (cyclase plus two subunits of the TAX-2/-4 CNGC), making them less versatile than ChR2.

Because no optogenetic silencing tool on the basis of transport or facilitation of K^+ currents in *C. elegans* exists, we characterized

two-component optogenetic systems, composed of a cNMP-gated channel and a PNC, for their potential to hyperpolarize BWM cells and/or cholinergic neurons. Here, the system composed of the cGMP-gated BeCNG1 channel and BeCyclOp was able to slightly hyperpolarize BWM cells. Its potential to hyperpolarize other cell types still has to be investigated. In case of the system comprising the cAMP-gated SthK channel, expression of the channel alone reduced the basal swimming frequency of the animals, independent of the cell type (muscle or cholinergic motor neurons), indicating a preactivation of the channel due to intrinsic cAMP. Also, co-expression with the PACs further reduced the basal swimming frequency (with the exception of BeCyclOp(A-3x) in BWMs), emphasizing the high affinity of SthK for cAMP, and a low dark activity of the PACs. Though the SthK-PAC system achieved strong and long-lasting hyperpolarizing effects, its applicability is restricted to cell types not containing intrinsic cAMP. To overcome this problem, SthK variants with specific mutations in the cAMP binding pocket might be helpful, to generate a channel with decreased cAMP affinity, that may then be used to obtain a more controllable tool for optogenetic silencing.

ACKNOWLEDGEMENTS

We thank Suely Gomes for providing the BeCNG1 plasmid. We acknowledge critical comments by members of the Gottschalk lab. We are indebted to H. Fettermann, F. Baumbach, R. Wagner for expert technical assistance, and F. Becker, W. Steuer Costa, A. Hammer, and N. Ho for technical help and help with data analysis. This work was funded by the Deutsche Forschungsgemeinschaft (DFG), grants SPP1926, CRC807, P11 and EXC115.

AUTHOR CONTRIBUTIONS

The experiments were conceived by T.H. and A.G., and performed by T.H. and A.P. who also analysed the data. Reagents were provided by J.N., S.Q., U.S., A.H., F.S.-W., P.H. and G.N. The paper was written by T.H. and A.G. Funding acquisition for, and supervision of, the project was provided by A.G.

CONFLICT OF INTEREST

The authors declare no conflicts of interest.

DECLARATION OF TRANSPARENCY AND SCIENTIFIC RIGOUR

This declaration acknowledges that this paper adheres to the principles for transparent reporting and scientific rigour of preclinical research as stated in the *BJP* guidelines for Design & Analysis and Immunoblotting and Immunochemistry, and as recommended by funding agencies, publishers, and other organizations engaged with supporting research.

DATA AVAILABILITY STATEMENT

The data are available on request from the authors.

ORCID

Shiqiang Gao https://orcid.org/0000-0001-6190-9443

Alexander Gottschalk https://orcid.org/0000-0002-1197-6119

REFERENCES

Alexander, S. P. H., Fabbro, D., Kelly, E., Mathie, A., Peters, J. A., Veale, E. L., Armstrong, J. F., Faccenda, E., Harding, S. D., Pawson, A. J., Sharman, J. L., Southan, C., Davies, J. A., & CGTP Collaborators. (2019). THE CONCISE GUIDE TO PHARMACOLOGY 2019/20: Enzymes. *British Journal of Pharmacology*, *176*, S297–S396. https://doi.org/10.1111/bph.14752

Alexander, S. P. H., Mathie, A., Peters, J. A., Veale, E. L., Striessnig, J., Kelly, E., Armstrong, J. F., Faccenda, E., Harding, S. D., Pawson, A. J., Sharman, J. L., Southan, C., Davies, J. A., & CGTP Collaborators. (2019). THE CONCISE GUIDE TO PHARMACOLOGY 2019/20: Ion channels. *British Journal of Pharmacology*, *176*, S142–S228. https://doi.org/10.1111/bph.14749

Avelar, G. M., Glaser, T., Leonard, G., Richards, T. A., Ulrich, H., & Gomes, S. L. (2015). A cyclic GMP-dependent K^+ channel in the blastocladiomycete fungus *Blastocladiella emersonii*. *Eukaryotic Cell*, *14*, 958–963. https://doi.org/10.1128/EC.00087-15

Avelar, G. M., Schumacher, R. I., Zaini, P. A., Leonard, G., Richards, T. A., & Gomes, S. L. (2014). A rhodopsin-guanylyl cyclase gene fusion functions in visual perception in a fungus. *Current Biology*, *24*, 1234–1240. https://doi.org/10.1016/j.cub.2014.04.009

Bargmann, C. I. (2006). Chemosensation in *C. elegans*. WormBook.

Bargmann, C. I., & Horvitz, H. R. (1991). Control of larval development by chemosensory neurons in *Caenorhabditis elegans*. *Science*, *251*, 1243–1246. https://doi.org/10.1126/science.2006412

Beck, S., Yu-Strzelczyk, J., Pauls, D., Constantin, O. M., Gee, C. E., Ehmann, N., Kittel, R. J., Nagel, G., & Gao, S. (2018). Synthetic light-activated ion channels for optogenetic activation and inhibition. *Frontiers in Neuroscience*, *12*, 643. https://doi.org/10.3389/fnins.2018.00643

Bergs, A., Schultheis, C., Fischer, E., Tsunoda, S. P., Erbguth, K., Husson, S. J., Govorunova, E., Spudich, J. L., Nagel, G., Gottschalk, A., & Liewald, J. F. (2018). Rhodopsin optogenetic toolbox v2.0 for light-sensitive excitation and inhibition in *Caenorhabditis elegans*. *PLoS One*, *13*, e0191802. https://doi.org/10.1371/journal.pone.0191802

Bernal Sierra, Y. A., Rost, B. R., Pofahl, M., Fernandes, A. M., Kopton, R. A., Moser, S., Holtkamp, D., Masala, N., Beed, P., Tukker, J. J., Oldani, S., Bönigk, W., Kohl, P., Baier, H., Schneider-Warme, F., Hegemann, P., Beck, H., Seifert, R., & Schmitz, D. (2018). Potassium channel-based optogenetic silencing. *Nature Communications*, *9*, 4611. https://doi.org/10.1038/s41467-018-07038-8

Birnby, D. A., Link, E. M., Vowels, J. J., Tian, H., Colacurcio, P. L., & Thomas, J. H. (2000). A transmembrane Guanylyl cyclase (DAF-11) and Hsp90 (DAF-21) regulate a common set of chemosensory behaviors in *Caenorhabditis elegans*. *Genetics*, *155*, 85–104.

Bock, A., Annibale, P., Konrad, C., Hannawacker, A., Anton, S. E., Maiellaro, I., Zabel, U., Sivaramakrishnan, S., Falcke, M., & Lohse, M. J. (2020). Optical mapping of cAMP signaling at the nanometer scale. *Cell*, *182*, 1519, e1517–1530.

Brams, M., Kusch, J., Spurny, R., Benndorf, K., & Ulens, C. (2014). Family of prokaryote cyclic nucleotide-modulated ion channels. *Proceedings of the National Academy of Sciences of the United States of America*, *111*, 7855–7860. https://doi.org/10.1073/pnas.1401917111

Brenner, S. (1974). The genetics of *Caenorhabditis elegans*. *Genetics*, *77*, 71–94. https://doi.org/10.1093/genetics/77.1.71

Buck, J., Sinclair, M. L., Schapal, L., Cann, M. J., & Levin, L. R. (1999). Cytosolic adenylyl cyclase defines a unique signaling molecule in mammals. *PNAS*, *96*, 79–84. https://doi.org/10.1073/pnas.96.1.79

Chow, B. Y., Han, X., Dobry, A. S., Qian, X., Chuong, A. S., Li, M., Henninger, M. A., Belfort, G. M., Lin, Y., Monahan, P. E., & Boyden, E. S. (2010). High-performance genetically targetable optical neural silencing by light-driven proton pumps. *Nature*, *463*, 98–102. https://doi.org/10.1038/nature08652

Chuong, A. S., Miri, M. L., Busskamp, V., Matthews, G. A. C., Acker, L. C., Sørensen, A. T., Young, A., Klapoetke, N. C., Henninger, M. A., Kodandaramaiah, S. B., Ogawa, M., Ramanlal, S. B., Bandler, R. C., Allen, B. D., Forest, C. R., Chow, B. Y., Han, X., Lin, Y., Tye, K. M., … Boyden, E. S. (2014). Noninvasive optical inhibition with a red-shifted microbial rhodopsin. *Nature Neuroscience*, *17*, 1123–1129. https://doi.org/10.1038/nn.3752

Cooper, D. M., & Tabbasum, V. G. (2014). Adenylate cyclase-centred microdomains. *The Biochemical Journal*, *462*, 199–213. https://doi.org/10.1042/BJ20140560

Cooper, D. M. F. (2003). Regulation and organization of adenylyl cyclases and cAMP. *The Biochemical Journal*, *375*, 517–529. https://doi.org/10.1042/bj20031061

Cosentino, C., Alberio, L., Gazzarrini, S., Aquila, M., Romano, E., Cermenati, S., Zuccolini, P., Petersen, J., Beltrame, M., van Etten, J., Christie, J. M., Thiel, G., & Moroni, A. (2015). Optogenetics engineering of a light-gated potassium channel. *Science*, *348*, 707–710. https://doi.org/10.1126/science.aaa2787

Curtis, M. J., Alexander, S., Cirino, G., Docherty, J. R., George, C. H., Giembycz, M. A., Hoyer, D., Insel, P. A., Izzo, A. A., Ji, Y., MacEwan, D. J., Sobey, C. G., Stanford, S. C., Teixeira, M. M., Wonnacott, S., & Ahluwalia, A. (2018). Experimental design and analysis and their reporting II: Updated and simplified guidance for authors and peer reviewers. *BJP*, *175*, 987–993. https://doi.org/10.1111/bph.14153

Edwards, S. L., Charlie, N. K., Milfort, M. C., Brown, B. S., Gravlin, C. N., Knecht, J. E., & Miller, K. G. (2008). A novel molecular solution for ultraviolet light detection in *Caenorhabditis elegans*. *PLoS Biology*, *6*, 0060198.

Etzl, S., Lindner, R., Nelson, M. D., & Winkler, A. (2018). Structure-guided design and functional characterization of an artificial red light-regulated guanylate/adenylate cyclase for optogenetic applications. *The Journal of Biological Chemistry*, *293*, 9078–9089. https://doi.org/10.1074/jbc.RA118.003069

Fielenbach, N., & Antebi, A. (2008). C. elegans dauer formation and the molecular basis of plasticity. *Genes & Development*, *22*, 2149–2165. https://doi.org/10.1101/gad.1701508

Fire, A. (1986). Integrative transformation of *Caenorhabditis elegans*. *The EMBO Journal*, *5*, 2673–2680. https://doi.org/10.1002/j.1460-2075.1986.tb04550.x

Fischer, E., Gottschalk, A., & Schuler, C. (2017). An optogenetic arrhythmia model to study catecholaminergic polymorphic ventricular tachycardia mutations. *Scientific Reports*, *7*, 17514. https://doi.org/10.1038/s41598-017-17819-8

Gao, S., Nagpal, J., Schneider, M. W., Kozjak-Pavlovic, V., Nagel, G., & Gottschalk, A. (2015). Optogenetic manipulation of cGMP in cells and animals by the tightly light-regulated guanylyl-cyclase opsin CyclOp. *Nature Communications*, *6*, 1–12.

Han, X., Qian, X., Bernstein, J. G., Zhou, H.-H., Franzesi, G. T., Stern, P., Bronson, R. T., Graybiel, A. M., Desimone, R., & Boyden, E. S. (2009). Millisecond-timescale optical control of neural dynamics in the non-human primate brain. *Neuron*, *62*, 191–198. https://doi.org/10.1016/j.neuron.2009.03.011

Houslay, M. D. (2010). Underpinning compartmentalised cAMP signalling through targeted cAMP breakdown. *Trends in Biochemical Sciences*, *35*, 91–100. https://doi.org/10.1016/j.tibs.2009.09.007

Husson, S. J., Costa, W. S., Wabnig, S., Stirman, J. N., Watson, J. D., Spencer, W. C., Akerboom, J., Looger, L. L., Treinin, M., Miller, D. M. III, Lu, H., & Gottschalk, A. (2012). Optogenetic analysis of a nociceptor neuron and network reveals ion channels acting downstream of primary sensors. *Current Biology*, *22*, 743–752. https://doi.org/10.1016/j.cub.2012.02.066

Husson, S. J., Liewald, J. F., Schultheis, C., Stirman, J. N., Lu, H., & Gottschalk, A. (2012). Microbial light-activatable proton pumps as neuronal inhibitors to functionally dissect neuronal networks in *C. elegans*. *PLoS One*, *7*, e40937. https://doi.org/10.1371/journal.pone.0040937

Kesters, D., Brams, M., Nys, M., Wijckmans, E., Spurny, R., Voets, T., Tytgat, J., Kusch, J., & Ulens, C. (2015). Structure of the SthK carboxy-terminal region reveals a gating mechanism for cyclic nucleotide-modulated ion channels. *PLoS One*, *10*, e0116369. https://doi.org/10.1371/journal.pone.0116369

Klapoetke, N. C., Murata, Y., Kim, S. S., Pulver, S. R., Birdsey-Benson, A., Cho, Y. K., Morimoto, T. K., Chuong, A. S., Carpenter, E. J., Tian, Z., Wang, J., Xie, Y., Yan, Z., Zhang, Y., Chow, B. Y., Surek, B., Melkonian, M., Jayaraman, V., Constantine-Paton, M., … Boyden, E. S. (2014). Independent optical excitation of distinct neural populations. *Nature Methods*, *11*, 338–346. https://doi.org/10.1038/nmeth.2836

Knopfel, T., Lin, M. Z., Levskaya, A., Tian, L., Lin, J. Y., & Boyden, E. S. (2010). Toward the second generation of optogenetic tools. *The Journal of Neuroscience*, *30*, 14998–15004. https://doi.org/10.1523/JNEUROSCI.4190-10.2010

Komatsu, H., Jin, Y.-H., L'Etoile, N., Mori, I., Bargmann, C. I., Akaike, N., & Ohshima, Y. (1999). Functional reconstitution of a heteromeric cyclic nucleotide-gated channel of *Caenorhabditis elegans* in cultured cells. *Brain Research*, *821*, 160–168. https://doi.org/10.1016/S0006-8993(99)01111-7

Liewald, J. F., Brauner, M., Stephens, G. J., Bouhours, M., Schultheis, C., Zhen, M., & Gottschalk, A. (2008). Optogenetic analysis of synaptic function. *Nature Methods*, *5*, 895–902. https://doi.org/10.1038/nmeth.1252

Linder, J. U. (2005). Substrate selection by class III adenylyl cyclases and guanylyl cyclases. *IUBMB Life*, *57*, 797–803. https://doi.org/10.1080/15216540500415636

Lucas, K. A., Pitari, G. M., Kazerounian, S., Ruiz-Stewart, I., Park, J., Schulz, S., Chepenik, K. P., & Waldman, S. A. (2000). Guanylyl cyclases and signaling by cyclic GMP. *Pharmacological Reviews*, *52*, 375–413.

Oranth, A., Schultheis, C., Tolstenkov, O., Erbguth, K., Nagpal, J., Hain, D., Brauner, M., Wabnig, S., Costa, W. S., McWhirter, R. D., Zels, S., Palumbos, S., Miller Iii, D. M., Beets, I., & Gottschalk, A. (2018). Food sensation modulates locomotion by dopamine and neuropeptide signaling in a distributed neuronal network. *Neuron*, *100*, 1414, e1410–1428. https://doi.org/10.1016/j.neuron.2018.10.024

Podda, M. V., & Grassi, C. (2014). New perspectives in cyclic nucleotide-mediated functions in the CNS: The emerging role of cyclic nucleotide-gated (CNG) channels. *Pflügers Archiv*, *466*, 1241–1257. https://doi.org/10.1007/s00424-013-1373-2

Ramot, D., MacInnis, B., & Goodman, M. (2008). Bidirectional temperature-sensing by a single thermosensory neuron in *C. elegans*. *Nature Neuroscience*, *11*, 908–915. https://doi.org/10.1038/nn.2157

Rost, B. R., Schneider-Warme, F., Schmitz, D., & Hegemann, P. (2017). Optogenetic tools for subcellular applications in neuroscience. *Neuron*, *96*, 572–603. https://doi.org/10.1016/j.neuron.2017.09.047

Ryu, M.-H., Kang, I.-H., Nelson, M. D., Jensen, T. M., Lyuksyutova, A. I., Siltberg-Liberles, J., Raizen, D. M., & Gomelsky, M. (2014). Engineering adenylate cyclases regulated by near-infrared window light. *Proceedings of the National Academy of Sciences of the United States of America*, *111*, 10167–10172. https://doi.org/10.1073/pnas.1324301111

Ryu, M.-H., Moskvin, O. V., Siltberg-Liberles, J., & Gomelsky, M. (2010). Natural and engineered photoactivated nucleotidyl cyclases for optogenetic applications. *The Journal of Biological Chemistry*, *285*, 41501–41508. https://doi.org/10.1074/jbc.M110.177600

Scheib, U., Broser, M., Constantin, O. M., Yang, S., Gao, S., Mukherjee, S., Stehfest, K., Nagel, G., Gee, C. E., & Hegemann, P. (2018). Rhodopsin-

cyclases for photocontrol of cGMP/cAMP and 2.3 Å structure of the adenylyl cyclase domain. *Nature Communications*, *9*, 2046. https://doi.org/10.1038/s41467-018-04428-w

Scheib, U., Stehfest, K., Gee, C. E., Korschen, H. G., Fudim, R., Oertner, T. G., & Hegemann, P. (2015). The rhodopsin-guanylyl cyclase of the aquatic fungus Blastocladiella emersonii enables fast optical control of cGMP signaling. *Science Signaling*, *8*, rs8. https://doi.org/10.1126/scisignal.aab0611

Schmidpeter, P. A. M., Gao, X., Uphadyay, V., Rheinberger, J., & Nimigean, C. M. (2018). Ligand binding and activation properties of the purified bacterial cyclic nucleotide-gated channel SthK. *The Journal of General Physiology*, *150*, 821–834. https://doi.org/10.1085/jgp.201812023

Schroder-Lang, S., Schwarzel, M., Seifert, R., Strunker, T., Kateriya, S., Looser, J., Watanabe, M., Kaupp, U. B., Hegemann, P., & Nagel, G. (2007). Fast manipulation of cellular cAMP level by light in vivo. *Nature Methods*, *4*, 39–42. https://doi.org/10.1038/nmeth975

Schuler, C., Fischer, E., Shaltiel, L., Steuer Costa, W., & Gottschalk, A. (2015). Arrhythmogenic effects of mutated L-type Ca^{2+}-channels on an optogenetically paced muscular pump in *Caenorhabditis elegans*. *Scientific Reports*, *5*, 14427. https://doi.org/10.1038/srep14427

Schultheis, C., Liewald, J. F., Bamberg, E., Nagel, G., & Gottschalk, A. (2011). Optogenetic long-term manipulation of behavior and animal development. *PLoS One*, *6*, e18766. https://doi.org/10.1371/journal.pone.0018766

Steuer Costa, W., Yu, S.-C., Liewald, J. F., & Gottschalk, A. (2017). Fast cAMP modulation of neurotransmission via neuropeptide signals and vesicle loading. *Current Biology: CB*, *27*, 495–507. https://doi.org/10.1016/j.cub.2016.12.055

Stierl, M., Stumpf, P., Udwari, D., Gueta, R., Hagedorn, R., Losi, A., Gärtner, W., Petereit, L., Efetova, M., Schwarzel, M., Oertner, T. G., Nagel, G., & Hegemann, P. (2011). Light modulation of cellular cAMP by a small bacterial photoactivated adenylyl cyclase, bPAC, of the soil bacterium *Beggiatoa*. *The Journal of Biological Chemistry*, *286*, 1181–1188. https://doi.org/10.1074/jbc.M110.185496

Stirman, J. N., Crane, M. M., Husson, S. J., Wabnig, S., Schultheis, C., Gottschalk, A., & Lu, H. (2011). Real-time multimodal optical control of neurons and muscles in freely behaving *Caenorhabditis elegans*. *Nature Methods*, *8*, 153–158. https://doi.org/10.1038/nmeth.1555

Sunahara, R. K., Beuve, A., Tesmer, J. J. G., Sprang, S. R., Garbers, D. L., & Gilman, A. G. (1998). Exchange of substrate and inhibitor specificities between adenylyl and guanylyl cyclases. *The Journal of Biological Chemistry*, *273*, 16332–16338. https://doi.org/10.1074/jbc.273.26.16332

Tanwar, M., Sharma, K., Moar, P., & Kateriya, S. (2018). Biochemical characterization of the engineered soluble photoactivated guanylate cyclases from microbes expands optogenetic tools. *Applied Biochemistry and Biotechnology*, *185*, 1014–1028. https://doi.org/10.1007/s12010-018-2710-x

Trieu, M. M., Devine, E. L., Lamarche, L. B., Ammerman, A. E., Greco, J. A., Birge, R. R., Theobald, D. L., & Oprian, D. D. (2017). Expression, purification, and spectral tuning of RhoGC, a retinylidene/guanylyl cyclase fusion protein and optogenetics tool from the aquatic fungus *Blastocladiella emersonii*. *The Journal of Biological Chemistry*, *292*, 10379–10389. https://doi.org/10.1074/jbc.M117.789636

Warr, W. A. (2012). Scientific workflow systems: Pipeline pilot and KNIME. *Journal of Computer-Aided Molecular Design*, *26*, 801–804. https://doi.org/10.1007/s10822-012-9577-7

Weissenberger, S., Schultheis, C., Liewald, J. F., Erbguth, K., Nagel, G., & Gottschalk, A. (2011). PACα—An optogenetic tool for in vivo manipulation of cellular cAMP levels, neurotransmitter release, and behavior in *Caenorhabditis elegans*. *Journal of Neurochemistry*, *116*, 616–625. https://doi.org/10.1111/j.1471-4159.2010.07148.x

Woldemariam, S., Nagpal, J., Hill, T., Li, J., Schneider, M. W., Shankar, R., Futey, M., Varshney, A., Ali, N., Mitchell, J., Andersen, K., Barsi-Rhyne, B., Tran, A., Costa, W. S., Krzyzanowski, M. C., Yu, Y. V., Brueggemann, C., Hamilton, O. S., Ferkey, D. M., … L'Etoile, N. (2019). Using a robust and sensitive GFP-based cGMP sensor for real-time imaging in intact *Caenorhabditis elegans*. *Genetics*, *213*, 59–77. https://doi.org/10.1534/genetics.119.302392

Yizhar, O., Fenno, L. E., Davidson, T. J., Mogri, M., & Deisseroth, K. (2011). Optogenetics in neural systems. *Neuron*, *71*, 9–34. https://doi.org/10.1016/j.neuron.2011.06.004

Zhang, F., Wang, L.-P., Brauner, M., Liewald, J. F., Kay, K., Watzke, N., Wood, P. G., Bamberg, E., Nagel, G., Gottschalk, A., & Deisseroth, K. (2007). Multimodal fast optical interrogation of neural circuitry. *Nature*, *446*, 633–639. https://doi.org/10.1038/nature05744

SUPPORTING INFORMATION

Additional supporting information may be found online in the Supporting Information section at the end of this article.

How to cite this article: Henß, T., Nagpal, J., Gao, S., Scheib, U., Pieragnolo, A., Hirschhäuser, A., Schneider-Warme, F., Hegemann, P., Nagel, G., & Gottschalk, A. (2021). Optogenetic tools for manipulation of cyclic nucleotides functionally coupled to cyclic nucleotide-gated channels. *British Journal of Pharmacology*, 1–19. https://doi.org/10.1111/bph.15445